








Article

Dynamics of MHD Convection of Walters B Viscoelastic Fluid through an Accelerating Permeable Surface Using the Soret–Dufour Mechanism

P. Anusha ¹, M. Naga Swapna Sri ¹, V.V. Venu Madhav ², Ch. Sri Chaitanya ², V.V. Spandana ³, Kuldeep K. Saxena ⁴, Dalael Saad Abdul-Zahra ⁵, Emanoil Linul ^{6,*}, Chander Prakash ^{7,8,*}, Dharam Budhi ⁹ and Raul Campilho ¹⁰

- ¹ Department of Mechanical Engineering, Prasad V. Potluri Siddhartha Institute of Technology, Kanuru, Vijayawada 520007, India
- ² Department of Mechanical Engineering, Velagapudi Ramakrishna Siddhartha Engineering College, Kanuru, Vijayawada 520007, India
- ³ Department of Health and Welfare, Guntur 522503, India
- ⁴ Department of Mechanical Engineering, GLA University, Mathura 281406, India
- ⁵ Department of Medical Physics, Hilla University College, Babylon 51002, Iraq
- ⁶ Department of Mechanics and Strength of Materials, Politehnica University Timisoara, 1 Mihai Viteazu Avenue, 300 222 Timisoara, Romania
- ⁷ School of Mechanical Engineering, Lovely Professional University, Phagwara 144411, India
- ⁸ Division of Research and Development, Lovely Professional University, Phagwara 144001, India
- ⁹ Division of Research & Innovation, Uttarakhand University, Dehradun 248007, India
- ¹⁰ Departamento de Engenharia Mecânica, Instituto Superior de Engenharia do Porto Rua Dr. Bernardino de Almeida, 4249-015 Porto, Portugal
- * Correspondence: emanoil.linul@upt.ro (E.L.); chander.mechengg@gmail.com (C.P.)



Citation: Anusha, P.; Sri, M.N.S.; Madhav, V.V.V.; Chaitanya, C.S.; Spandana, V.V.; Saxena, K.K.; Abdul-Zahra, D.S.; Linul, E.; Prakash, C.; Budhi, D.; et al. Dynamics of MHD Convection of Walters B Viscoelastic Fluid through an Accelerating Permeable Surface Using the Soret–Dufour Mechanism. *Appl. Sci.* **2022**, *12*, 9431. <https://doi.org/10.3390/app12199431>

Academic Editor: Kambiz Vafai

Received: 7 August 2022

Accepted: 3 September 2022

Published: 20 September 2022

Publisher's Note: MDPI stays neutral with regard to jurisdictional claims in published maps and institutional affiliations.



Copyright: © 2022 by the authors. Licensee MDPI, Basel, Switzerland. This article is an open access article distributed under the terms and conditions of the Creative Commons Attribution (CC BY) license (<https://creativecommons.org/licenses/by/4.0/>).

Abstract: The MHD convective Walters-B memory liquid flow past a permeable accelerating surface with the mechanism of Soret-Dufour is considered. The flow equation constitutes a set of partial differential equations (PDEs) to elucidate the real flow of a non-Newtonian liquid. The radiation thermo-physical parameters were employed based on the use of Roseland approximation. This implies the fluid employed in this exploration is optically thick. Utilizing suitable similarity terms, the flow equation PDEs were simplified to become total differential equations. The spectral homotopy analysis method (SHAM) was utilized to provide outcomes to the model. The SHAM involves the addition of the Chebyshev pseudospectral approach (CPM) alongside the homotopy analysis approach (HAM). The outcomes were depicted utilizing graphs and tables for the quantities of engineering concern. The mechanisms of Soret and Dufour were separately examined. The imposed magnetism was found to lessen the velocity plot while the thermal radiation term elevates the temperature plot because of the warm particles of the fluid.

Keywords: Soret and Dufour influence; free convection; Walters-B memory; permeable surface; SHAM; MHD; magnetic field

1. Introduction

Mixed convective flow has been of great importance and has attracted the attention of many researchers in recent decades because of its importance in the field of engineering and environmental and geophysical applications. In view of these applications and the importance of Soret and Dufour for fluids that have a light molecular weight, as well as fluids with a medium molecular weight, investigators have published many works. Alam et al. [1] examined the contribution of Soret together with Dufour on free convection MHD as well as mass transport flow using a numerical approach. Mahdy [2] performed a non-similar boundary layer analysis to examine the contribution of Soret together with Dufour with heat plus mass transport for a power-law non-Newtonian liquid. Thermal

diffusion means that heat transport is induced using a concentration gradient, while diffusion-thermo refers to mass diffusion, which is induced using a thermal gradient. The problem of mixed convective flow together with incompressible flow under the impact of buoyancy plus transverse magnetism simultaneously with Dufour–Soret has been investigated by Makinde [3]. Cheng [4] elucidated the contribution of Soret together with Dufour to mixed convection heat, together with mass transport through a downward-pointing vertical wall. Heat and mass movement of the natural convection motion in a saturated penetrable channel with Soret–Dufour, as well as variable viscosity, was analyzed by Moorthy and Senthilvadivay [5]. Sharma et al. [6] explored Soret together with Dufour on mixed convection MHD plus unsteadiness motion past a radiative porous vertical plate. Seini and Makinde [7] numerically solved the simultaneous contribution of Soret and Dufour on a mixed convection flow by elucidating viscous together with ohmic dissipation. Uwanta and Halima [8] examined how Soret and Dufour behave in the exploration of heat together with mass transportation with viscous dissipation plus constant suction. Aruna et al. [9] extensively discussed the effects of adding Soret to Dufour in the model of unsteady mixed convection MHD heat alongside mass motion. Tella et al. [10] explored the Soret–Dufour phenomenon in their study of viscous as well as chemically reactive fluid.

The elucidation of Walters-B liquid flow has been considered in most recent published research because of its various applications in food processing industries and technology. The flow of such fluids has been studied by Joneidi et al. [11] whose model involved a vertical channel together with a penetrable wall. Kumar [12] solely presented work on viscoelastic liquid in a penetrable channel. Vijaya et al. [13] studied viscoelastic fluid thermal convection flow through a porous channel and Biot number influence. In another development, the study of Walters-B liquid flow through porous and tapered asymmetric channels was elucidated by Abdukhadi and Tamara. Pandey et al. [14] explored the behavior of Walters-B liquid in a nanofluid layer that is heated at the bottom. Moatimid and Hassan [15] presented non-Newtonian Walters-B term flow in a nanofluid vertical layer. Islam and Haque [16] studied Walters-B memory flow with a radiative and induced magnetic field. Rana and Chand [17] studied elastico-viscous and Walters-B nanofluid layers as well as Rayleigh–Benard convection. Hayat et al. [18] investigated the behavior of homogeneous, together with heterogeneous, reactions on Oldroyd-B fluid flow.

Alam et al. [1] investigated free convection MHD together with the mass flow of a viscous chemical reacting together with an electrically conducting fluid. Moorthy et al. [19] analyzed heat together with the mass transport of natural convection by considering variable viscosity as well as Soret–Dufour effects. Regarding heat together with the mass transport of two-dimensional and steady free convection MHD motion with viscous dissipation, Soret–Dufour was studied by Lavanya and Ratnam [20]. Reddy et al. [21] explained the behavior of thermal radiation, as well as MHD mixed convection flow, by considering oscillatory suction. Krishna et al. [22] explored the convective motion of an incompressible viscous plus chemically reacting fluid with a heat source. The results of diluted convective heat together with mass motion in a Darcy with pores were elucidated by Srinivasacharya et al. [23].

Spectral techniques have become important tools for scientist and engineers in providing solution to systems of differential equations. The spectral techniques are known for their elegance, accuracy, and lower computational analysis time. SHAM combines CPM with HAM. SHAM was explained by Motsa et al. [24,25] in solving nonlinear ordinary differential equations. After his introduction of SHAM, many researchers have used it in solving boundary layer problem. Motsa et al. [26] presented the use of SHAM in solving PDEs. Bivariate SHAM for the outcome of heat together with the mass transport of boundary layer motion was elucidated by Motsa and Makukula [27]. Fagbade et al. [28] used SHAM in solving the problem of MHD natural convection Walters-B liquid flow.

Motsa et al. [29] presented an improved SHAM for solving boundary layer motion problems. Among other authors that have used SHAM in the literature discussed in this work are Khidir and Sibanda [30], Fagbade et al. [31], Mehmood et al. [32], Walter et al. [33],

Liao et al. [34], Canuto et al. [35], Fornberg et al. [36], Trefethen et al. [37] etc. Authors who worked extensively on nano fluids and fluid behavior in multiple conditions include Doaa Rizk et al. [38], Asad Ullah et al. [39], Shahid Khan et al. [40], Khan et al. [41], Rashid Nawaz et al. [42], and Zahir Shah et al. [43].

In all the above-mentioned works, little or no attention has been given to elucidating the steady MHD convective motion of Walters-B term liquid past an accelerating porosity surface with the consideration of Soret together with Dufour. SHAM is utilized to obtain the numerical solution of the nonlinear ODE. This work is necessary because the results obtained will be useful for engineers in the industry, especially in the food processing industry. The rest of this work is organized as follows: The mathematical formulation is presented in Section 2 and the numerical solution using SHAM is presented in Section 3. We elucidate the outcomes and discussions in Section 4, and the final remarks of the findings are made in Section 5.

2. Model Equations

We considered a problem of steady, laminar, and viscous, as well as two-dimensional MHD mixed convection motion, of Walters-B liquid flow. The x -axis is considered an upward surface in a vertical area; likewise, the y -axis is considered normal to fluid motion. In the model, heat source/absorption and thermal radiation together with viscous dissipation is taken into consideration. Magnetism $B(x)$ is imposed transversely to fluid flow toward the y -axis. The Joule heating effect is neglected in the energy equation, while the chemical reaction influence is neglected in the concentration equation. However, concentration and temperature gradients are so high that Soret, as well as Dufour, effects cannot be neglected. The velocity and temperature together with species concentration given by $U_w(x, y)$, $T_w(x, y)$, $C_w(x, y)$ are functions of x and y . In this analysis, all attributes of fluid are presumed uniform, with density variations in the momentum flow equation as an exceptional case.

We consider in our study the flow equations for Walters-B viscoelastic liquid because it involves one parameter of fluid. The tensor S of the liquid follows the following equations by Mehmood [32] and Walter [33].

$$S = -PI + \tau \tag{1}$$

where p = pressure, I = identity tensor and

$$\tau = 2\eta_0 e - 2k_0 \frac{\delta e}{\delta t} \tag{2}$$

where e = the rate of strain tensor given as:

$$2e = \nabla(v) + \nabla(v)^T \tag{3}$$

where v means velocity, ∇ = gradient operator, $\frac{\delta}{\delta t}$ = the tensor quantity of the convected differentiation subject to motion material, η_0 = the viscosity limit at a small shear rate, and k_0 = the short relaxation time. Hence, η_0 and k_0 are expressed as:

$$\eta_0 = \int_0^\infty \lambda(\xi) d\xi, \quad k_0 = \int_0^\infty \tau \lambda(\xi) d\xi \tag{4}$$

where $\lambda(\xi)$ is the relaxation spectrum, by Walters [33]. The rate of the stream tensor differential term $\frac{\delta e}{\delta t}$ in Equation (2) is expressed as:

$$\frac{\delta e}{\delta t} = \frac{\partial e}{\partial t} + v \cdot \nabla(e) - e \cdot \nabla(v) - (\nabla(v))^T \cdot e \tag{5}$$

The model in this study is based on Walters-B liquid fluid approximation, considering that the relaxation time is short in such a way that any terms involving

$$\int_0^\infty \tau^n \lambda(\tau) d\tau \quad n \geq 2 \tag{6}$$

have been forgone.

Because of the simplifications above on the Walters-B model and the assumptions together with Boussinesq’s evaluation, the model analysis, which is presented in Figure 1 of the present investigation, is:

$$\frac{\partial u}{\partial x} + \frac{\partial v}{\partial y} = 0 \tag{7}$$

$$\left| \begin{matrix} u & -v \\ \frac{\partial u}{\partial y} & \frac{\partial u}{\partial x} \end{matrix} \right| + \left| \begin{matrix} -nu & -u \\ \frac{\sigma \beta_0^2(x)}{\rho} & \frac{\partial^2 u}{\partial y^2} \end{matrix} \right| + \left| \begin{matrix} -g & \\ \beta_c(C - C_\infty) & \beta_t(T - T_\infty) \end{matrix} \right| + K_0 \left[\left| \begin{matrix} v & u \\ \frac{\partial^3 u}{\partial y^2 \partial x} & -\frac{\partial^3 u}{\partial y^3} \end{matrix} \right| + \left| \begin{matrix} \frac{\partial u}{\partial x} & \frac{\partial u}{\partial y} \\ \frac{\partial^2 v}{\partial y^2} & -\frac{\partial^2 u}{\partial y^2} \end{matrix} \right| \right] = 0 \tag{8}$$

$$\left| \begin{matrix} u & -v \\ \frac{\partial T}{\partial y} & \frac{\partial T}{\partial x} \end{matrix} \right| + \left| \begin{matrix} \frac{1}{\rho c_p} & \alpha \\ \frac{\partial^2 T}{\partial y^2} & \frac{\partial q_r}{\partial y} \end{matrix} \right| + \left| \begin{matrix} -\frac{\mu}{\rho c_p} & \frac{Dk_T}{c_s c_p} \\ \frac{\partial^2 C}{\partial y^2} & \left(\frac{\partial u}{\partial y}\right)^2 \end{matrix} \right| - \frac{Q_0}{\rho c_p} (T - T_\infty) = 0 \tag{9}$$

$$\left| \begin{matrix} u & -v \\ \frac{\partial C}{\partial y} & \frac{\partial C}{\partial x} \end{matrix} \right| + \left| \begin{matrix} -D & \frac{Dk_T}{T_m} \\ \frac{\partial^2 T}{\partial y^2} & \frac{\partial^2 C}{\partial y^2} \end{matrix} \right| = 0 \tag{10}$$

with the boundary constraint:

$$u(x, 0) = ax, \quad v(x, 0) = v_w, \quad T(x, 0) = T_w(x) = T_0 + A_0x \tag{11}$$

$$C(x, 0) = C_w(x) = C_0 + M_0x, \quad u(x, \infty) = 0, \quad T(x, \infty) = T_0, \quad C(x, \infty) = C_0 \tag{12}$$

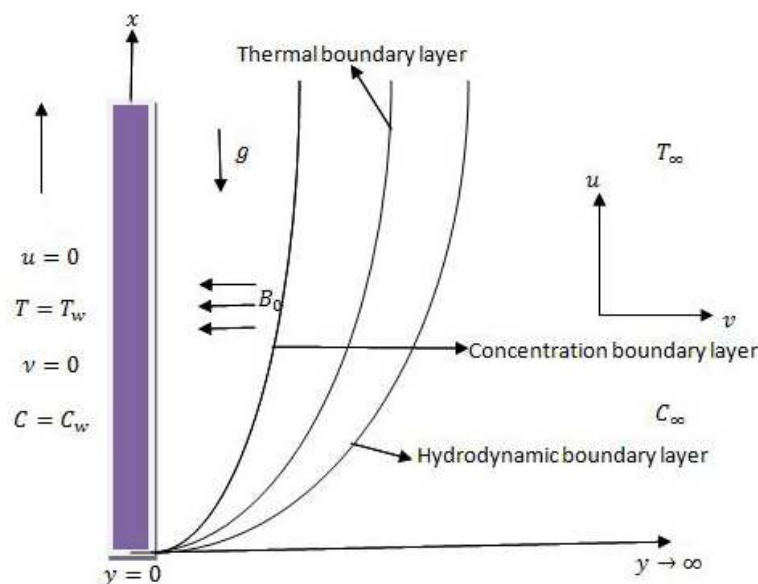


Figure 1. Flow configurations.

Employing the Roseland model, considering the heat flux as:

$$q_r = -\frac{4\sigma^*}{3k^*} \frac{\partial T^4}{\partial y} \tag{13}$$

Assuming the difference between the temperatures when flow region is small and T^4 implies a linear parameter of T_∞ , we simplified T^4 by expanding Taylor’s series about T_∞ as well as avoiding higher terms. The process of Taylor’s series expansion is given below:

$$f(T) = f(T_\infty) + (T - T_\infty)f'(T_\infty) + \frac{(T - T_\infty)^2}{2!}f''(T_\infty) + \dots$$

where

$$f(T) = T^4, \text{ then } f'(T) = 4T^3, \text{ } f''(T) = 12T^2$$

which implies that

$$f(T_\infty) = T_\infty^4, \text{ then } f'(T_\infty) = 4T_\infty^3, \text{ } f''(T_\infty) = 12T_\infty^2$$

Evaluating the above, as well as avoiding a higher term, we have

$$T^4 \approx 4T_\infty^3 T - 3T_\infty^4 \tag{14}$$

Substituting Equation (14) into (13) and using the result on the second term at RHS of the energy equation gives

$$-\frac{1}{\rho c_p} \frac{\partial q_r}{\partial y} = \frac{16\sigma^* T_\infty^3}{3\rho c_p k^*} \frac{\partial T}{\partial y} \tag{15}$$

Using the above simplification on energy Equation (8), we have:

$$u \frac{\partial T}{\partial x} + v \frac{\partial T}{\partial y} = \alpha \frac{\partial^2 T}{\partial y^2} + \frac{16\sigma^* T_\infty^3}{3\rho c_p k^*} \frac{\partial T}{\partial y} + \frac{\mu}{\rho c_p} \left(\frac{\partial u}{\partial y^2} \right)^2 + \frac{Q_0}{\rho c_p} (T - T_\infty) + \frac{Dk_T}{c_s c_p} \frac{\partial^2 C}{\partial y^2} \tag{16}$$

To evaluate the flow equations into coupled ODE, the following similarity terms are introduced:

$$\varphi = \sqrt{vax}f(\eta), \quad \eta = \sqrt{\frac{a}{v}}y, \quad u = \frac{\partial \varphi}{\partial y}, \quad v = -\frac{\partial \varphi}{\partial x} \tag{17}$$

$$T = T_\infty + (T_w - T_\infty)\vartheta(\eta), \quad C = C_\infty + (C_w - C_\infty)\phi(\eta) \tag{18}$$

The stream function defined above is found to satisfy the continuity Equation (7). Introducing the similarity transformation above on the governing Equations (7)–(12), the fourth-order coupled ODEs are derived:

$$\beta f \frac{d^4 f}{d\eta^4} + \frac{d^3 f}{d\eta^3} - M^2 \frac{df}{d\eta} - \left| \frac{f}{\frac{df}{d\eta}} \frac{-\frac{df}{d\eta}}{\frac{d^2 f}{d\eta^2}} \right| + \beta \left| \frac{-2\frac{df}{d\eta}}{\frac{d^2 f}{d\eta^2}} \frac{-\frac{d^2 f}{d\eta^2}}{\frac{d^3 f}{d\eta^3}} \right| + Gt\vartheta + Gm\phi = 0 \tag{19}$$

$$\left(\frac{1 + R}{Pr} \right) \frac{d^2 \vartheta}{d\eta^2} + \left| \frac{f}{\vartheta} \frac{-\frac{df}{d\eta}}{\frac{d\vartheta}{d\eta}} \right| + Ec \frac{d^2 f}{d\eta^2} \frac{d^2 f}{d\eta^2} + \alpha \vartheta + Df \frac{d^2 \phi}{d\eta^2} = 0 \tag{20}$$

$$\frac{1}{Sc} \frac{d^2 \phi}{d\eta^2} + \left| \frac{f}{\phi} \frac{-\frac{df}{d\eta}}{\frac{d\phi}{d\eta}} \right| + Sr \frac{d^2 \phi}{d\eta^2} = 0 \tag{21}$$

subject to

$$\frac{df}{d\eta} = 1, \quad f = S_w, \quad \vartheta = 1, \quad \phi = 1 \text{ at } \eta = 0 \tag{22}$$

$$\frac{df}{d\eta}(\infty) \rightarrow 0, \quad \vartheta(\infty) \rightarrow 0, \quad \phi(\infty) \rightarrow 0 \text{ as } \eta \rightarrow \infty \tag{23}$$

where $\beta = \frac{ak_0}{v\rho}$ is the viscoelastic parameter, $M = \left(\frac{\sigma\beta_0^2}{\rho a} \right)^{\frac{1}{2}}$ represents the magnetic term, $Gt = \frac{g\beta(T_w - T_\infty)}{a^2 x}$ represents the Grashof number, $Gm = \frac{g\beta^*(C_w - C_\infty)}{a^2 x}$ means represents the

Grashof number, $R = \frac{16\sigma T_\infty^3}{3k^*k}$ represents thermal radiation, $Pr = \frac{\nu}{\alpha}$ represents the Prandtl number, $Ec = \frac{ax}{c_p(T_w - T_\infty)}$ represents the Eckert number, $\alpha = \frac{Q_0}{\rho c_p a}$ represents the heat generation or absorption term, and $Sc = \frac{\nu}{D}$ represents the Schmidt number.

3. Numerical Approach: SHAM

SHAM is a version of HAM that numerically solves problems of heat together with mass transport. Detailed steps and explanations of HAM can be found in Liao [34] who was credited for proposing the method. SHAM, as proposed by Motsa et al. [35,36], uses CSC to decompose the deformation higher-order HAM in a case whereby the nonlinear differential equations cannot be solved analytically. Therefore, SHAM combines CSC with HAM to solve boundary layer equations. SHAM considered that the linear operator is employed to develop an algorithm that selects the entire linear part of the flow equations. It leads to a tedious sequence of linear ODE, which can be solved numerically using SHAM. Due to the elegance and high accuracy achieved by the spectral methods with few grid points [37–39], it has become a major tool for scientists and engineers in solving nonlinear differential equations. To apply SHAM, the problem-simplified domain is changed from $[0, 1]$ to $[-1, 1]$ for an easy model. Furthermore, the boundary constraints are explored homogeneously using the following functions:

$$\xi = \frac{2\eta}{L} - 1, \quad \xi \in [-1, 1], \quad f(\eta) = f(\xi) + f_0(\eta), \quad \vartheta(\eta) = \vartheta(\xi) + \vartheta_0(\eta), \quad \phi(\eta) = \phi(\xi) + \phi_0(\eta) \tag{24}$$

where $f_0(\eta)$, $\vartheta_0(\eta)$ and $\phi_0(\eta)$ are initial approximations constraints:

$$f_0(\eta) = -f_w + 1 - e^{-\eta}, \quad \vartheta_0(0) = \phi_0(0) = e^{-\eta} \tag{25}$$

By substituting Equations (24) and (25) into the simplified governing Equations (19)–(21), it gives

$$f'''' - 2\beta f' f'''' + a_1 f' + a_2 f'''' + \beta f'' f'' + a_3 f'' - M^2 f' + \beta f f'''' + a_4 f + a_5 f'''' + Gt\vartheta - ff'' + a_6 f + a_7 f'' + Gm\phi - f' f' + a_8 f' = J_1(\eta) \tag{26}$$

$$(1 + R)\vartheta'' + Prf\vartheta' + b_1 f + b_2 \vartheta' + \alpha\vartheta - Prf'\vartheta + b_3 f' + b_4 \vartheta + PrEf'' f'' + b_5 f'' + DfPr\phi'' = J_2(\eta) \tag{27}$$

$$\phi'' + Scf\phi' + c_1 f + c_2 \phi' + ScSr\vartheta'' - Scf'\phi + c_3 f' + c_4 \phi = J_3(\eta) \tag{28}$$

subject to:

$$f'(-1) = f'(1) = 0 \quad f(-1) = 0, \quad \vartheta(-1) = \vartheta(1) = 0, \quad \phi(-1) = \phi(1) \tag{29}$$

where the prime in Equations (26)–(29) denotes differentiation *w.r.t* ξ , and we have set

$$b_1 = Pr\vartheta_0, b_2 = Prf_0, b_3 = -Pr\vartheta_0, b_4 = Prf'_0, b_5 = 2PrEf''_0, a_1 = -2\vartheta f''_0, a_2 = -2\beta f'_0, a_3 = 2\beta f''_0, a_4 = \beta f''''_0(\beta), a_5 = \beta f_0, a_6 = -f''_0, a_7 = -f_0, a_8 = -2f'_0, c_1 = Sc\phi'_0, c_2 = Scf_0, c_3 = -Sc\phi_0, c_4 = -Scf'_0 \tag{30}$$

$$J_1(\eta) = -f''''_0 + 2\beta f'_0 f''''_0 - \beta f''_0 f''_0 + M^2 f'_0 - \beta f_0 f''''_0 - Gt\vartheta_0 + f_0 f''_0 - Gm\phi_0 - f'_0 f'_0 \tag{31}$$

$$J_2(\eta) = -(1 + R)\vartheta''_0 - Prf_0\vartheta'_0 - \alpha\vartheta_0 + Prf'_0\vartheta_0 - PrEf''_0 f''_0 - PrDf\phi''_0 \tag{32}$$

$$J_3(\eta) = -\phi''_0 - Scf_0\phi'_0 - ScSr\vartheta''_0 + Scf'_0\phi_0 \tag{33}$$

where f_0, ϑ_0 , and ϕ_0 are functions of η . The linear part of Equations (26)–(28) is given by:

$$f''''_l + a_1 f'_l + a_2 f''''_l + a_3 f''_l - M^2 f'_l + a_4 f_l + a_5 f''''_l + Gt\vartheta_l + a_6 f_l + a_7 f''_l + Gm\phi_l + a_8 f'_l = J_1(\eta) \tag{34}$$

$$(1 + R)\vartheta''_l + b_1f_l + b_2\vartheta'_l + \alpha\vartheta_l + b_3f'_l + b_4\vartheta_l + b_5f''_l + DfPr\phi''_l = J_2(\eta) \tag{35}$$

$$\phi''_l + c_1f_l + c_2\phi'_l + ScSr\vartheta''_l + c_3f'_l + c_4\phi_l = J_3(\eta) \tag{36}$$

subject to

$$f_l(-1) = f'_l(1) = 0, \quad \vartheta_l(-1) = \vartheta_l(1) = 0, \quad \phi_l(-1) = \phi_l(1) = 0 \tag{37}$$

CPm is used to obtain the solution to Equations (34)–(37), and we further approximate functions $f_l(\zeta), \vartheta_l(\zeta)$ together with ϕ_l as a series of truncations using Chebyshev polynomials given as:

$$f_l(\zeta) \sim f_l^N(\zeta_j) + \sum_{k=0}^N \bar{f}_k T_{1k}(\zeta_j), \quad j = 0, \dots, N \tag{38}$$

$$\vartheta_l(\zeta) \sim \vartheta_l^N(\zeta_j) + \sum_{k=0}^N \bar{\vartheta}_k T_{2k}(\zeta_j), \quad j = 0, \dots, N \tag{39}$$

$$\phi_l(\zeta) \sim \phi_l^N(\zeta_j) + \sum_{k=0}^N \bar{\phi}_k T_{3k}(\zeta_j), \quad j = 0, \dots, N \tag{40}$$

T_{1k}, T_{2k} and T_{3k} represent the k th polynomial with $\zeta_0, \zeta_1, \dots, \zeta_N =$ collocation region of Gauss-Lobatto given as:

$$\zeta_j = \cos\left(\frac{\pi j}{N}\right), \quad j = 0, 1, \dots, N \tag{41}$$

where $N =$ collocation numeric points and $f_l(\zeta), \vartheta_l(\zeta)$ and $\phi_l(\zeta)$ are derivatives within the collocation point, given by:

$$\frac{d^r f_l}{d\zeta^r} = \sum_{k=0}^N D_{kj} f_l(\zeta_j), \quad \frac{d^r \vartheta_l}{d\zeta^r} = \sum_{k=0}^N D_{kj} \vartheta_l(\zeta_j), \quad \frac{d^r \phi_l}{d\zeta^r} = \sum_{k=0}^N D_{kj} \phi_l(\zeta_j) \tag{42}$$

where $r =$ the differentiation order and $D =$ the spectral differentiation matrix. Using Equations (38)–(40) on Equations (34)–(36) yields

$$AF_L = G \tag{43}$$

subject to

$$f_l(\zeta_N) = -S_w, \quad \sum_{k=0}^N D_{0,m} f_l(\zeta_m) = 1, \quad \vartheta_l(\zeta_N) = \phi_l(\zeta_N) = 1, \quad \vartheta_l(\zeta_0) = \vartheta_l(\zeta_0) = 0 \tag{44}$$

where

$$A = \begin{bmatrix} A_{11} & A_{12} & A_{13} \\ A_{21} & A_{22} & A_{23} \\ A_{31} & A_{32} & A_{33} \end{bmatrix} \tag{45}$$

and

$$\begin{aligned} A_{11} &= D^3 + a_1D + a_2D^3 + a_3D^2 - M^2D + a_4 + a_5D^4 + a_6 + a_7D^2 + a_8D \\ A_{12} &= GtI, \quad A_{13} = GmI, \quad A_{21} = b_1 + b_3D + b_5D^2, \quad A_{22} = (1 + R)D^2 + b_2D + \alpha + b_4 \\ A_{23} &= DfPrD^2, \quad A_{31} = c_1 + c_3D, \quad A_{32} = ScSrD^2, \quad A_{33} = D^2 + c_2D + c_4 \\ F_L &= [f_l(\zeta_0, \dots, \zeta_N), \vartheta_l(\zeta_0, \dots, \zeta_N), \phi_l(\zeta_0), \dots, \phi_l(\zeta_N)]^T \\ G &= [H_1(\eta_0), H_1(\eta_1, \dots, \eta_N), H_2(\eta_0), H_2(\eta_1), \dots, H_2(\eta_N), H_3(\eta_0), H_3(\eta_1, \dots, \eta_N)] \\ a_i &= \text{diag}([a_i(\eta_0), a_i(\eta_1, \dots, \eta_{N-1})]) \\ b_i &= \text{diag}([b_i(\eta_0), b_i(\eta_1), \dots, b_i(\eta_{N-1})]) \\ c_i &= \text{diag}([c_i(\eta_0), c_i(\eta_1, \dots, \eta_{N-1})]), \quad i = 1, 2, 3, 4, 5, 6, 7, 8 \end{aligned}$$

where T represents transpose, $diag$ represents the matrix diagonal, and I represents the matrix identity of magnitude $(N + 1) \times (N + 1)$. To use the constraints in (44), we first eliminate the first rows and columns together with the last rows with columns of A . In the same vein, we delete the first rows together with the last rows of $f_l(\xi), \theta_l(\xi), \vartheta_l(\xi)$ and G . The conditions in (44) is further utilized on the first rows together with the last rows of matrix A , which is a reframed matrix. Finally, we set the first rows as well as the last rows of matrix G (modified version) to be zeros. Thus, the values of $f_l(\xi_0), \dots, f_l(\xi_N), \vartheta_l(\xi_0), \dots, \vartheta_l(\xi_N), \phi_l(\xi_0), \dots, \phi_l(\xi_N)$ can be determined from

$$F_L = A^{-1}G \tag{46}$$

Equation (46) provides the initial function to determine the SHAM outcome of the flow model. Hence, to find the SHAM outcomes of (26)–(28), it requires that we define the linear operator:

$$L_f[\bar{f}(\eta; q), \bar{\vartheta}(\eta; q), \bar{\phi}(\eta; q)] = f'''_l + a_1 f'_l + a_2 f'''_l + a_3 f''_l - M^2 f'_l + a_4 f_l + a_5 f''''_l + Gt\vartheta_l + a_6 f_l + a_7 f''_l + Gm\phi_l + a_8 f'_l \tag{47}$$

$$L_\vartheta[\bar{f}(\eta; q), \bar{\vartheta}(\eta; q), \bar{\phi}(\eta; q)] = (1 + R)\vartheta''_l + b_1 f_l + b_2 \vartheta'_l + \alpha \vartheta_l + b_3 f'_l + b_4 \vartheta_l + b_5 f''_l + DfPr\vartheta''_l \tag{48}$$

$$L_\phi[\bar{f}(\eta; q), \bar{\vartheta}(\eta; q), \bar{\phi}(\eta; q)] = \phi''_l + c_1 f_l + c_2 \phi'_l + ScSr\vartheta''_l + c_3 f'_l + c_4 \phi_l \tag{49}$$

In the above equations, $q \in [0, 1]$ = functions embedded and $\bar{f}(\eta; q), \bar{\vartheta}(\eta; q)$ and $\bar{\phi}(\eta; q)$ are undetermined terms. The deformation zero equation is expressed as:

$$(1 - q)L_{\bar{f}}[\bar{f}(\eta; q) - \bar{f}_0(\eta)] = qh_{\bar{f}}H_{\bar{f}}(\eta)N_{hf}[\bar{f}(\eta; q), \bar{\vartheta}(\eta; q), \bar{\phi}(\eta; q)] \tag{50}$$

$$1(-q)L_{\bar{\vartheta}}[\bar{\vartheta}(\eta; q) - \bar{\vartheta}_0(\eta)] = qh_{\bar{\vartheta}}H_{\bar{\vartheta}}(\eta)N_{h\vartheta}[\bar{f}(\eta; q), \bar{\vartheta}(\eta; q), \bar{\phi}(\eta; q)] \tag{51}$$

$$1(-q)L_{\bar{\phi}}[\bar{\phi}(\eta; q) - \bar{\phi}_0(\eta)] = qh_{\bar{\phi}}H_{\bar{\phi}}(\eta)N_{h\phi}[\bar{f}(\eta; q), \bar{\vartheta}(\eta; q), \bar{\phi}(\eta; q)] \tag{52}$$

In the above equations, $h_{\bar{f}}, h_{\bar{\vartheta}}$ and $h_{\bar{\phi}}$ = nonzero convergence controlling auxiliary parameters, and $N_{hf}, N_{h\vartheta}, N_{h\phi}$ = nonlinear operators defined by:

$$N_{hf}[\bar{f}(\eta; q), \bar{\vartheta}(\eta; q), \bar{\phi}(\eta; q)] = \bar{f}'''' + a_1 \bar{f}' - 2\beta \bar{f}' \bar{f}'''' + a_2 \bar{f}'''' + a_3 \bar{f}'' - M^2 \bar{f}' + a_4 \bar{f} + \beta \bar{f}'' \bar{f}'' + a_5 \bar{f}'''' + Gt\bar{\vartheta} + \beta \bar{f} \bar{f}'''' + a_6 \bar{f} + a_7 \bar{f}'' - \bar{f} \bar{f}'' + Gm\bar{\phi} + a_8 \bar{f}' - \bar{f}' \bar{f}' \tag{53}$$

$$N_{h\vartheta}[\bar{f}(\eta; q), \bar{\vartheta}(\eta; q), \bar{\phi}(\eta; q)] = (+R)\vartheta'' + Pr\bar{f}\vartheta' + b_1 \bar{f} + b_2 \vartheta' + \alpha \bar{\vartheta} - Pr\bar{f}'\bar{\vartheta} + b_3 \bar{f}' + b_4 \bar{\vartheta} + PrE\bar{f}''\bar{f}'' + b_5 \bar{f}'' + DfPr\bar{\phi}'' \tag{54}$$

$$N_{h\phi}[\bar{f}(\eta; q), \bar{\vartheta}(\eta; q), \bar{\phi}(\eta; q)] = \bar{\phi}'' + Sc\bar{f}\bar{\phi}' + c_1 \bar{f} + c_2 \bar{\phi}' + ScSr\bar{\vartheta}'' - Sc\bar{f}'\bar{\phi} + c_3 \bar{f}' + c_4 \bar{\phi} \tag{55}$$

Differentiating (50)–(52) m times *w.r.t.* q and taking $q = 0$ and dividing the outcome expressions by $m!$, we obtain the m th deformation order equations:

$$L_{\bar{f}}[\bar{f}(\xi) - \chi_m \bar{f}_{m-1}(\xi)] = h_{\bar{f}}(\xi) \bar{R}_m^{\bar{f}}(\xi) \tag{56}$$

$$L_{\bar{\vartheta}}[\bar{\vartheta}(\xi) - \chi_m \bar{\vartheta}_{m-1}(\xi)] = h_{\bar{\vartheta}}(\xi) \bar{R}_m^{\bar{\vartheta}}(\xi) \tag{57}$$

$$L_{\bar{\phi}}[\bar{\phi}(\xi) - \chi_m \bar{\phi}_{m-1}(\xi)] = h_{\bar{\phi}}(\xi) \bar{R}_m^{\bar{\phi}}(\xi) \tag{58}$$

subject to:

$$\bar{f}_m(-1) = \bar{\vartheta}_m(-1) = \bar{\phi}_m(-1) = 0, \quad \bar{f}'_m(1) = \bar{\vartheta}'_m(1) = \bar{\phi}'_m(1) = 0 \tag{59}$$

where

$$R_m^f(\xi) = \bar{f}_{m-1} + a_1 \bar{f}'_{m-1} + a_2 \bar{f}''_{m-1} + a_3 \bar{f}'''_{m-1} + a_4 \bar{f}_{m-1} - M^2 \bar{f}'_{m-1} + a_5 \bar{f}''''_{m-1} + Gt \bar{\theta}_{m-1} + a_6 \bar{f}_{m-1} + a_7 \bar{f}''_{m-1} + Gm \bar{\phi}_{m-1} + a_8 \bar{f}'_{m-1} + \sum_{n=0}^{m-1} \left(-2\beta \bar{f}'_n \bar{f}'''_{m-1-n} + \beta \bar{f}''_n \bar{f}''_{m-1-n} + \beta \bar{f}_n \bar{f}''''_{m-1-n} - \bar{f}_n \bar{f}''_{m-1-n} - \bar{f}'_n \bar{f}'_{m-1-n} \right) - H_1(\eta)1(-\chi_m) \tag{60}$$

$$R_m^\theta(\xi) = (+R) \bar{\theta}''_{m-1} + b_1 \bar{f}_{m-1} + b_2 \bar{\theta}'_{m-1} + \alpha \bar{\theta}_{m-1} + b_3 \bar{f}'_{m-1} + b_4 \bar{\theta}_{m-1} + b_5 \bar{f}''_{m-1} + Pr Df \bar{\phi}''_{m-1} + \sum_{n=0}^{m-1} \left(Pr \bar{f}_n \bar{\theta}'_{m-1-n} - Pr \bar{f}'_n \bar{\theta}_{m-1-n} + Pr E \bar{f}''_n \bar{f}''_{m-1-n} \right) - H_2(\eta)1(-\chi_m) \tag{61}$$

$$R_m^\phi(\xi) = \bar{\phi}''_{m-1} + c_1 \bar{f}_{m-1} + c_2 \bar{\phi}'_{m-1} + Sc Sr \bar{\theta}''_{m-1} + c_3 \bar{f}'_{m-1} + c_4 \bar{\phi}_{m-1} + \sum_{n=0}^{m-1} \left(Sc \bar{f}_n \bar{\phi}'_{m-1-n} - Sc \bar{f}'_n \bar{\phi}_{m-1-n} \right) - H_3(\eta)1(-\chi_m) \tag{62}$$

4. Results and Discussion

Equations (18)–(20) subject to constraints (21) and (22) have been numerically addressed utilizing SHAM for all controlling terms such as the viscoelastic term (β), Magnetism term (M), thermal Grashof (Gt), mass Grashof (Gm), thermal radiation term (R), Prandtl (Pr), Eckert (E), heat generation/absorption parameter (α), Dufour number (Df), suction/injection velocity (Sw), Schmidt (Sc), and Soret term (Sr). SHAM combines the Chebyshev pseudospectral techniques with HAM in solving differential equations. Throughout our computational analysis, we employ $M = 1.0$, $Gt = 2.0$, $R = 0.5$, $Pr = 0.71$, $E = 0.01$, $Sw = 0.1$, $\alpha = 0.01$, $\beta = 0.01$, $Sr = 0.2$ and $Df = 0.3$, $Sc = 0.61$ to compute tables and plot graphs, unless stated otherwise.

Figure 2 explains the contribution of the thermal radiation term on the velocity, concentration, and temperature plots. Thermal radiation boasts convective flow as an upsurge in thermal radiation causes a significant elevation in the fluid velocity together with temperature. This ascension is shown in Figure 2a,b because, as thermal radiation increases, the velocity plus temperature plot increases.

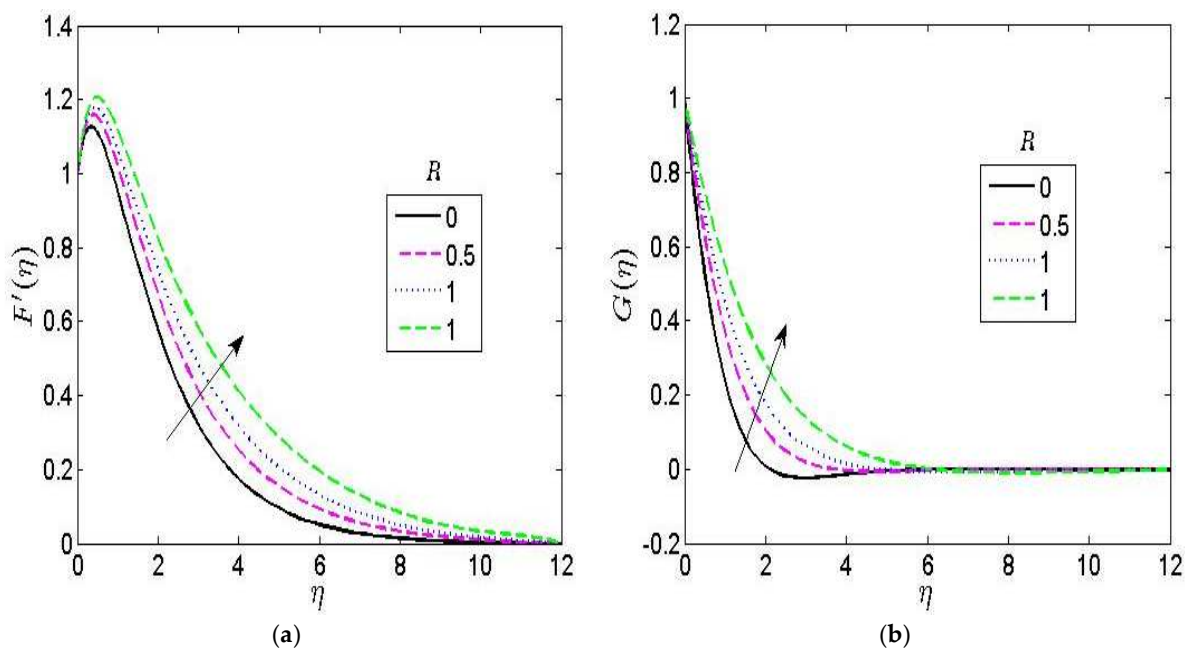


Figure 2. Effect of thermal radiation R on (a) velocity and (b) temperature profiles.

Figure 3 represents the contribution of the magnetic term to the velocity, concentration, and temperature plot. From Figure 3a, it is seen that increases in the magnetic term produces a reduction in the velocity profile. This is owing to the fact the Lorentz force produced by the applied magnetism strength in the direction of the flow. In Figure 3b,c, it observed that an increase in the magnetism term increases the temperature and concentration plots.

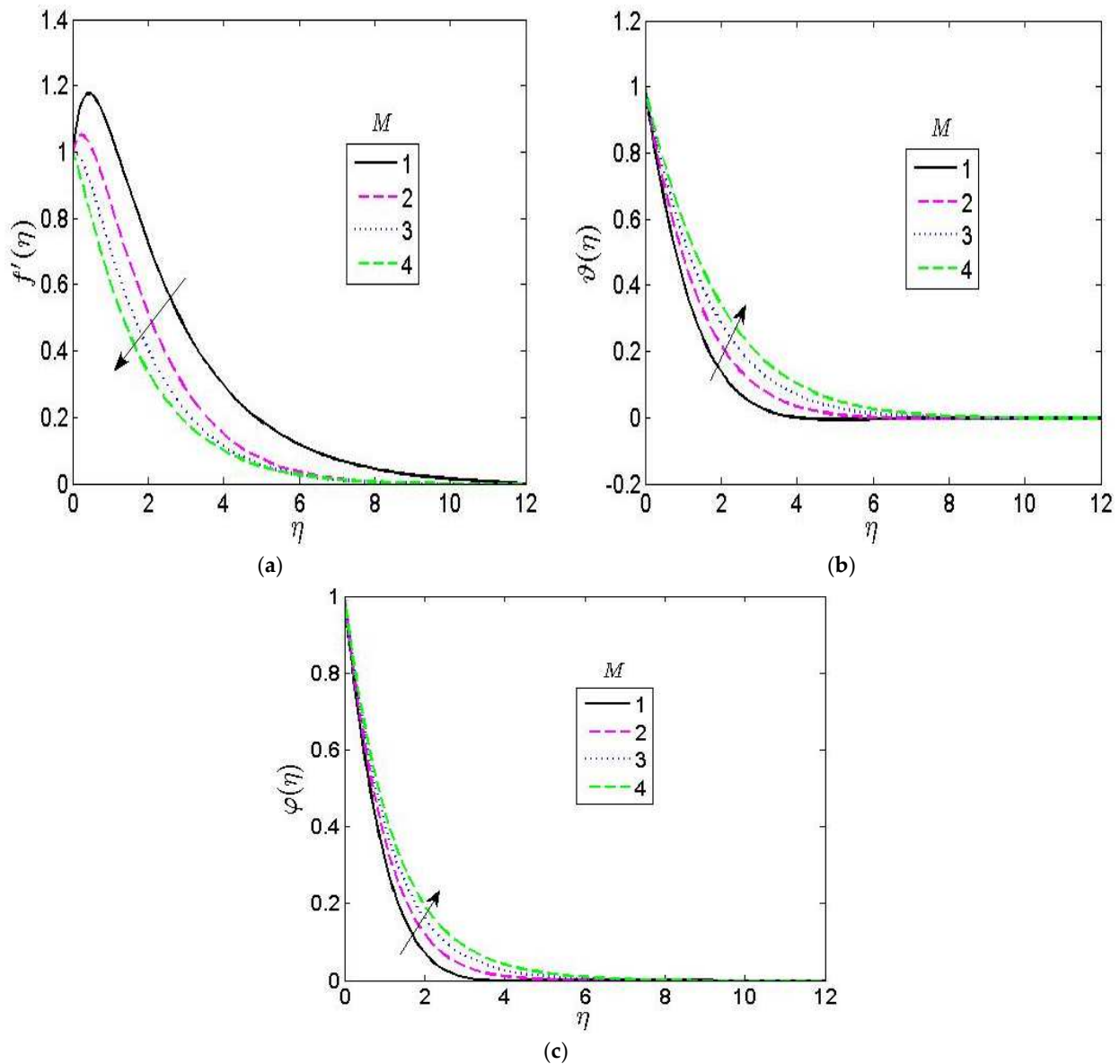


Figure 3. Effect of magnetic parameter M on (a) velocity, (b) temperature, and (c) concentration profiles.

Prandtl number behavior is elucidated in Figure 4. It is noticeable that an increase in Prandtl (Pr) reduces the velocity and temperature profiles. This is because small values of Pr lead to elevation in thermal conductivities, which causes heat to diffuse out of the heated plate faster than when the Pr number is high. It is noted that when the Prandtl number is small (meaning $Pr < 1$), the fluid will be conductive.

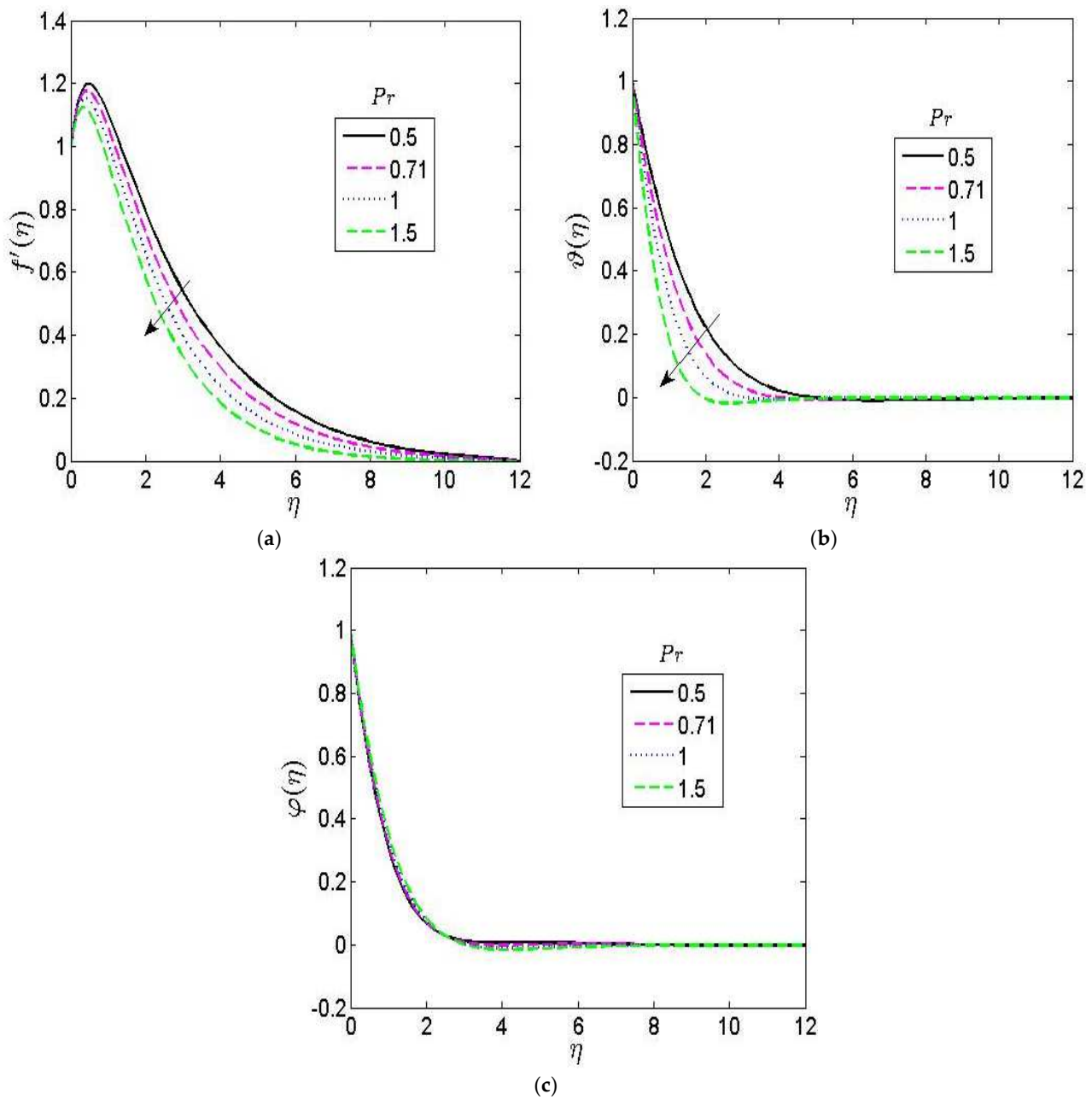


Figure 4. Effect of Prandtl number Pr on (a) velocity, (b) temperature, and (c) concentration profiles.

Figure 5 represents the contribution of the viscous/energy term (i.e., Eckert) on temperature and velocity, as well as concentration distributions. The viscous/energy dissipation represents the relationship existing between the kinetic energy of fluid movement and the enthalpy. It is obvious from Figure 5a,b that as the Eckert number increases, elevation in the velocity and temperature of the fluid is observed.

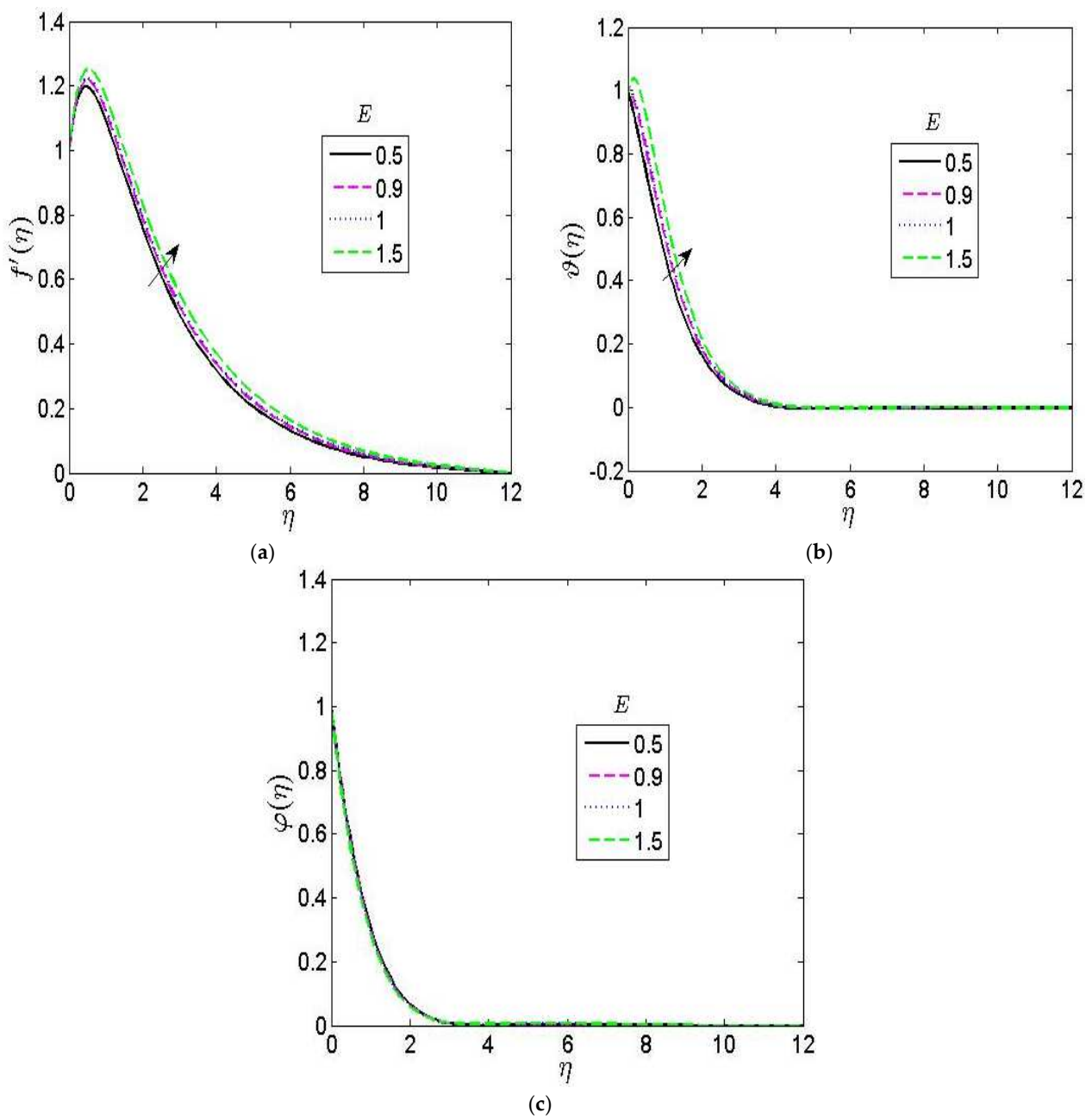


Figure 5. Effect of Eckert number E on (a) velocity, (b) temperature, and (c) concentration profiles.

Figure 6 exhibits the velocity, concentration, and temperature plots for distinct numbers of Schmidt (Sc). Sc defined the quotient of momentum over mass diffusivity. Thus, in Figure 6c, a decrease in the concentration distribution is observed when Sc is increased. In fact, it shows that larger values of Sc are equivalent to very small mass diffusivity. In Figure 6a, a degeneration in the fluid velocity is noted when Sc is increased.

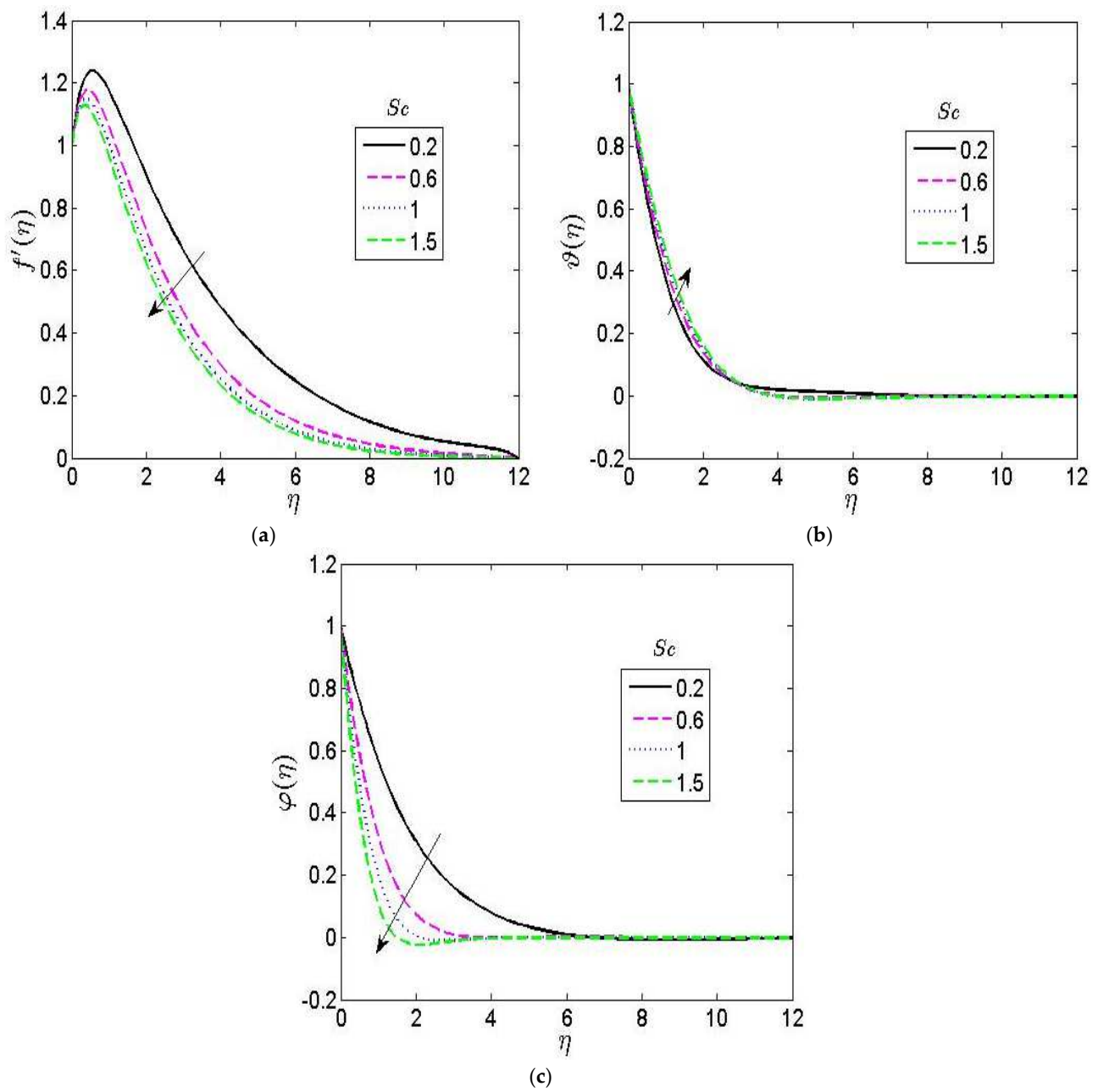


Figure 6. Effect of Schmidt number Sc on (a) velocity, (b) temperature, and (c) concentration profiles.

The influence of suction velocity (Sw) is explored in Figure 7. It is noticeable that acceleration in the suction velocity causes an elevation in the velocity, as well as temperature at the plate, but decreases when it is further from the plate as shown in Figure 7a,b. Moreover, from Figure 7c, an elevation in the concentration can be observed when the suction velocity is higher.

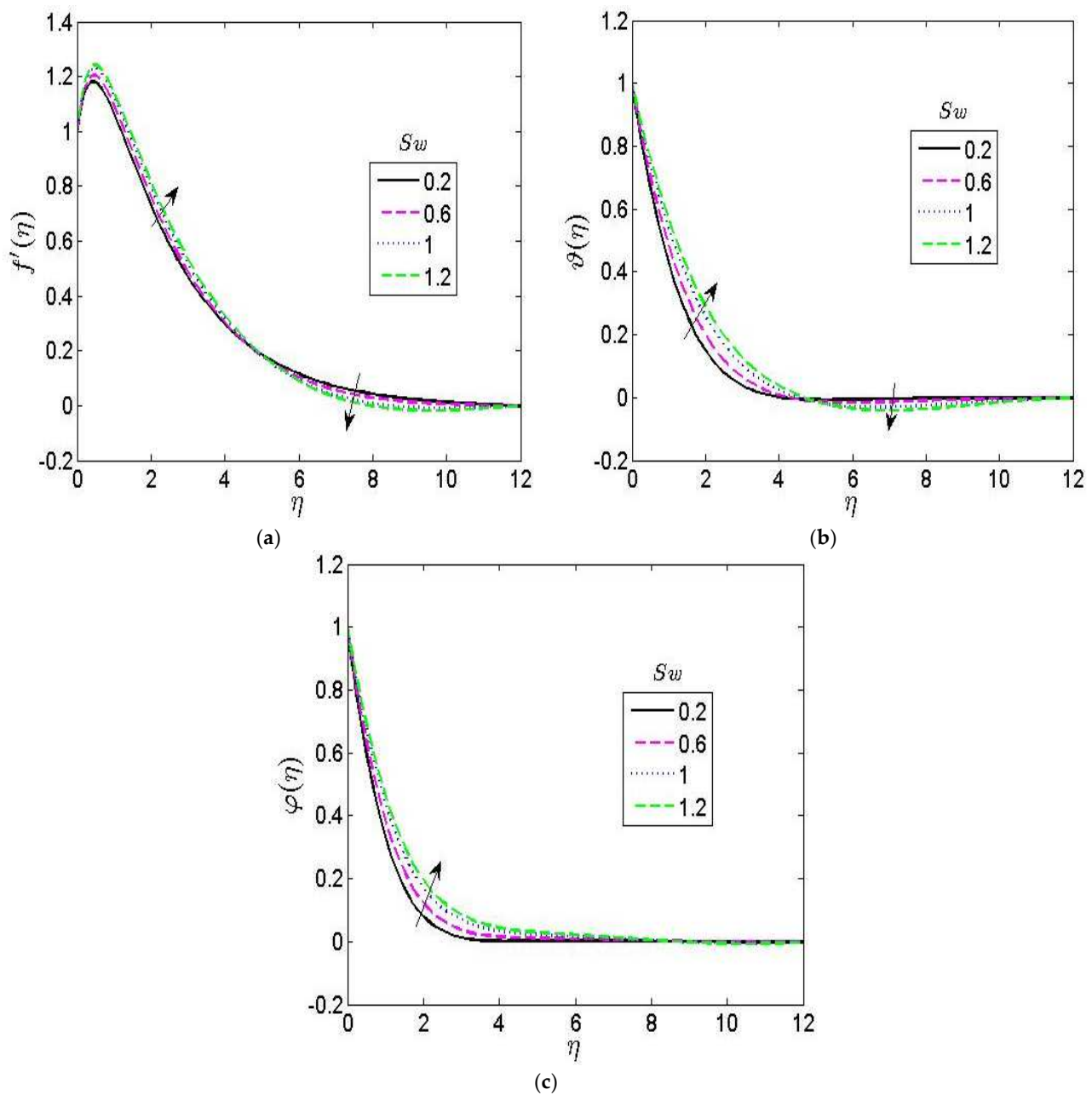


Figure 7. Effect of suction velocity S_w on (a) velocity, (b) temperature, and (c) concentration profiles.

The contribution of Dufour and Soret is explained separately for thorough investigations. We plotted the contribution of Dufour on the velocity, concentration, and temperature graphs in Figure 8. It is noticed that the Dufour or diffusion thermal parameter alters the temperature. From Figure 8a, as the Dufour parameter is intensified, the fluid velocity increases, whereas Figure 8b shows that a higher value of the Dufour term produces an acceleration in the fluid temperature. In the same vein, the effect of Dufour on the fluid concentration is very minimal, as shown in Figure 8c.

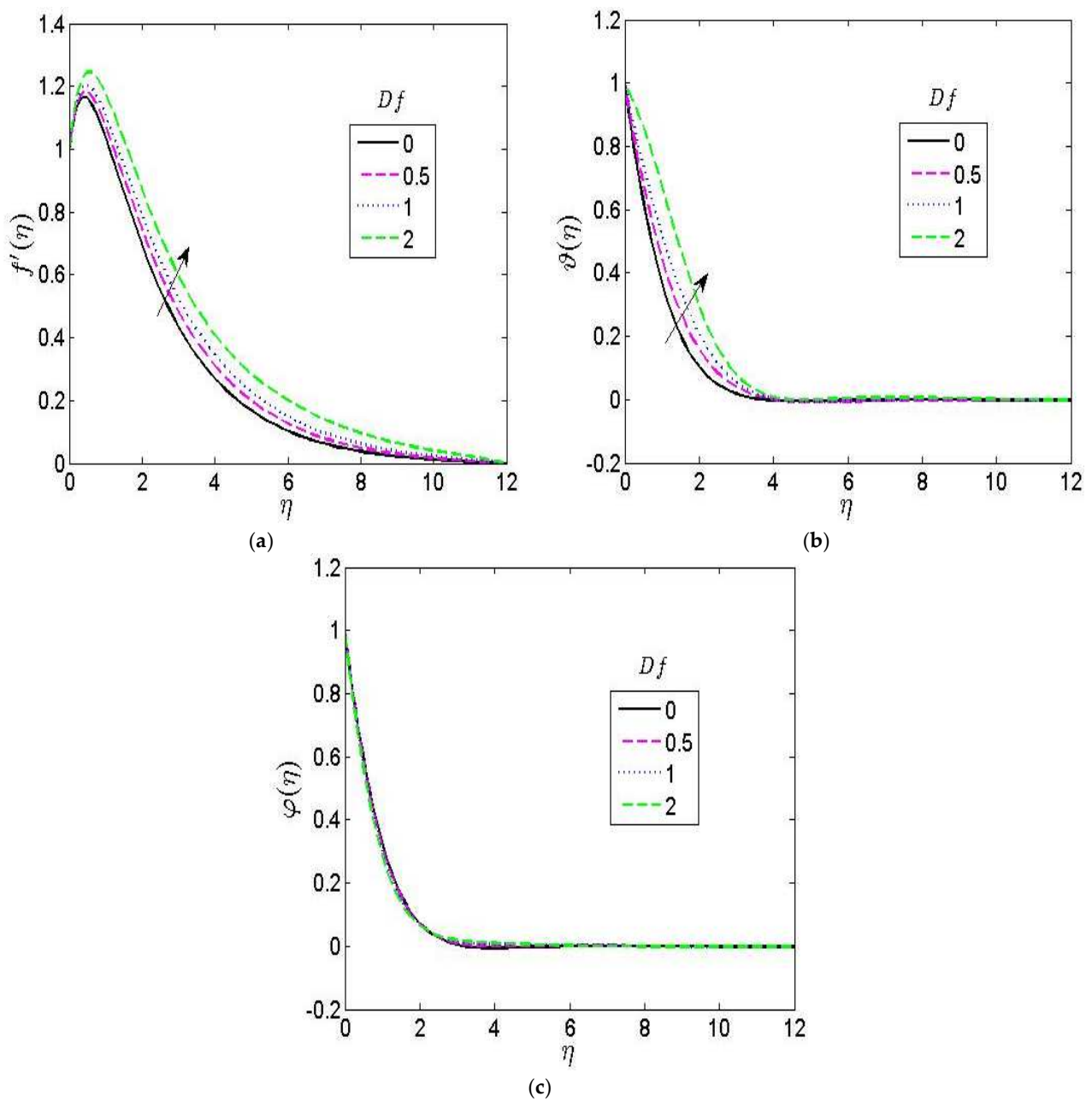


Figure 8. Effect of Dufour parameter Df on (a) velocity, (b) temperature, and (c) concentration profiles.

Figure 9 represents the consideration of a distinct Soret number in the concentration, velocity, and temperature plots. Figure 9c shows that an increment in the Soret term produces an acceleration in the concentration plot, as expected. In Figure 9a, an increase in the velocity graph is detected with a higher value of the Soret term. We observed that the contribution of the Soret term (Sr) and Dufour parameter (Df) on the temperature and concentration plot is opposite.

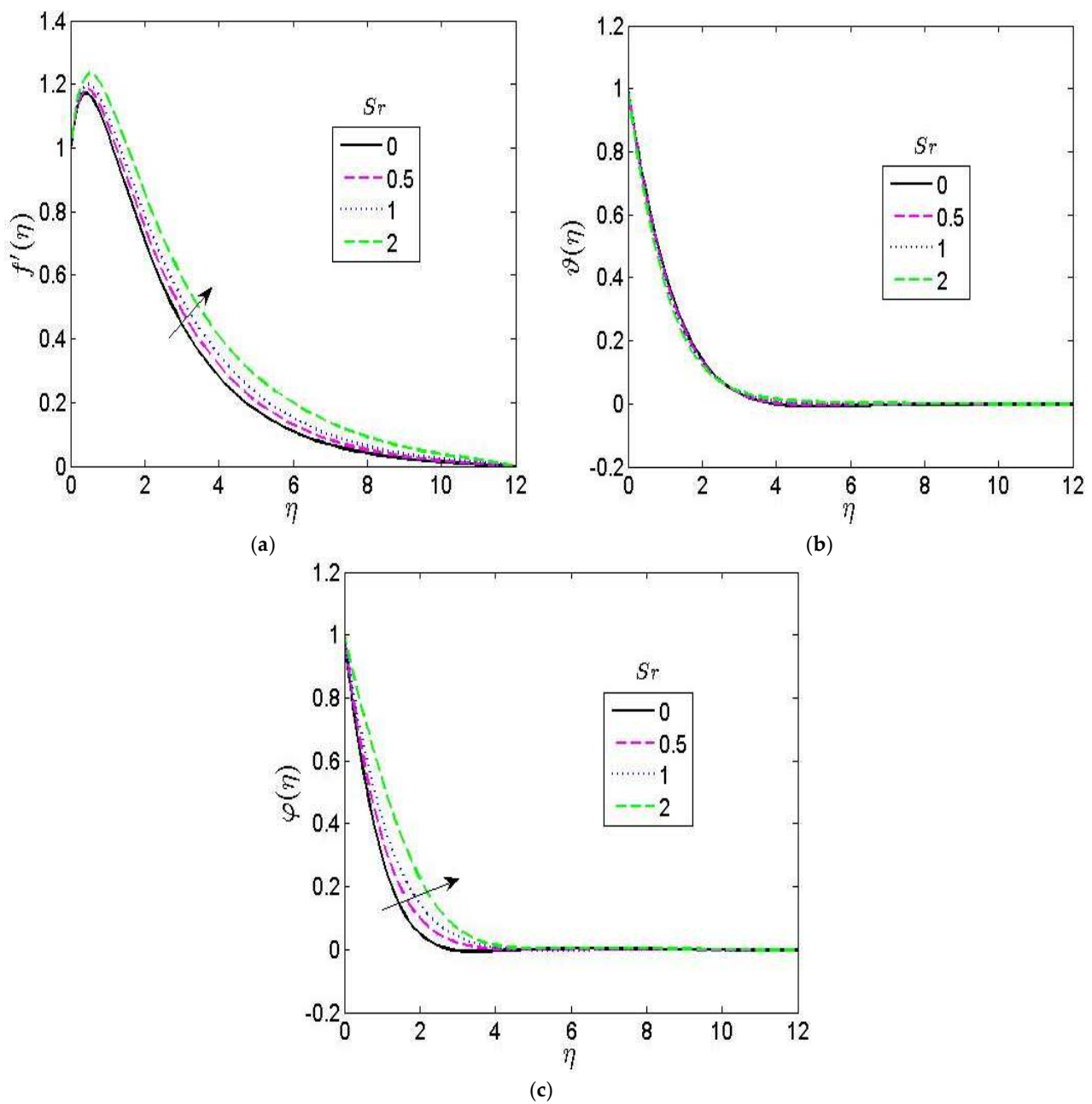


Figure 9. Effect of Soret parameter Sr on (a) velocity, (b) temperature, and (c) concentration profiles.

The contribution of the viscoelastic term (β) (i.e., Weissenberg numeric) is plotted in Figure 10. The viscoelastic parameter β describes the influence of the coefficient of normal stress on the motion. Figure 10a portrays the contribution of the viscoelastic term on the velocity graph. It is detected from the graph that at any moment in the flow regime, an increase in β produces a drastic degeneration in the velocity of the fluid, whereas we observed in this study that a higher value of the viscoelastic term has no contribution to the temperature and concentration plot as depicted in Figure 10b,c. The result in Figure 10a signifies that a higher value of β has the tendency to decrease the hydrodynamics layer thickness.

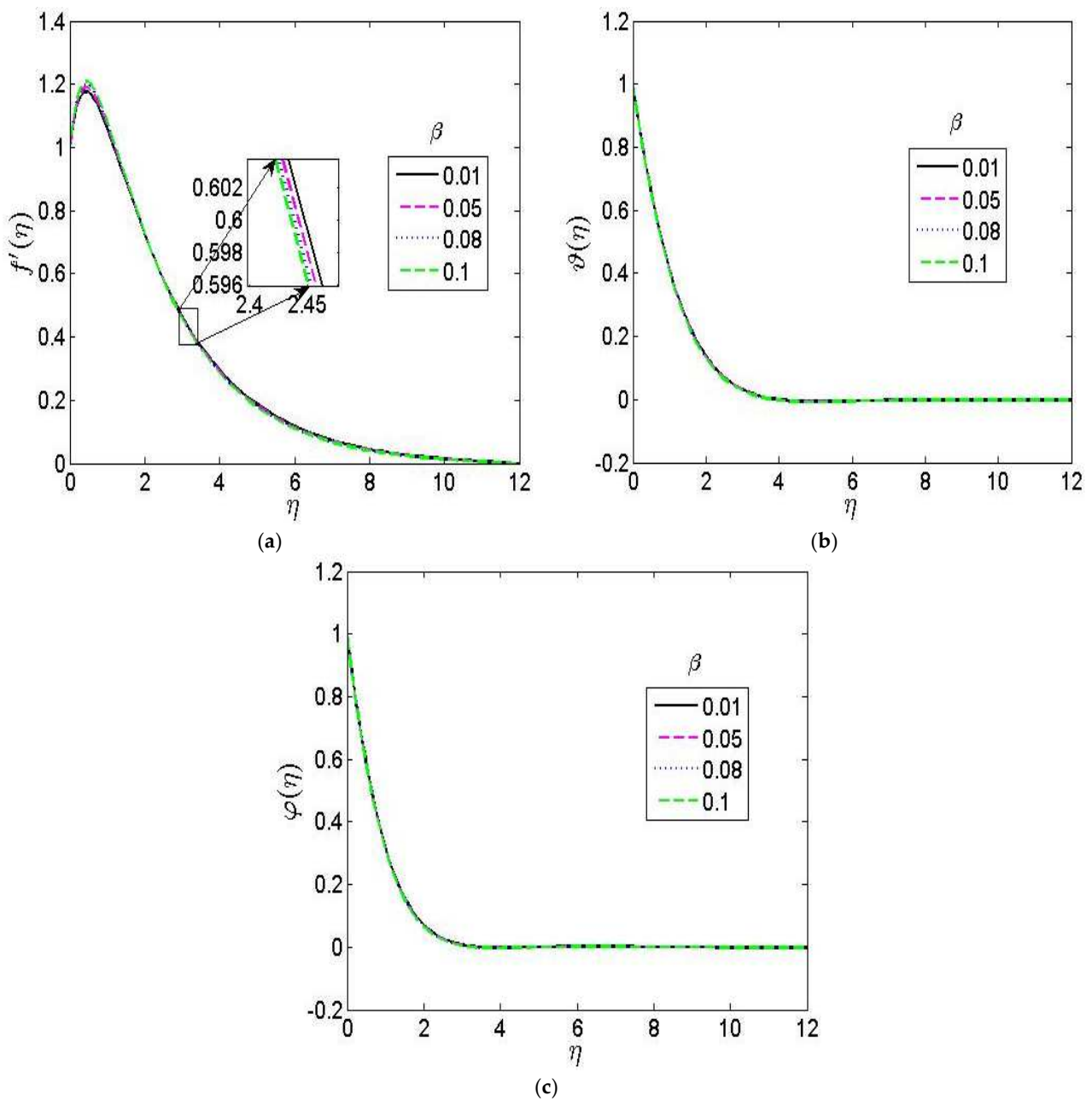


Figure 10. Effect of Weissenberg number β on (a) velocity, (b) temperature, and (c) concentration profiles.

We plotted the contribution of the heat absorption/generation term (α) on the velocity, concentration, and temperature distributions in Figure 11. It is detected from Figure 11a,b that a higher α produces an acceleration in the fluid velocity and temperature. This signifies that temperature together with velocity in the boundary layer increases when $\alpha > 0$ while the reverse is the case when $\alpha < 0$. Thus, when $\alpha > 0$, more heat is generated and the temperature within the layer is enhanced.

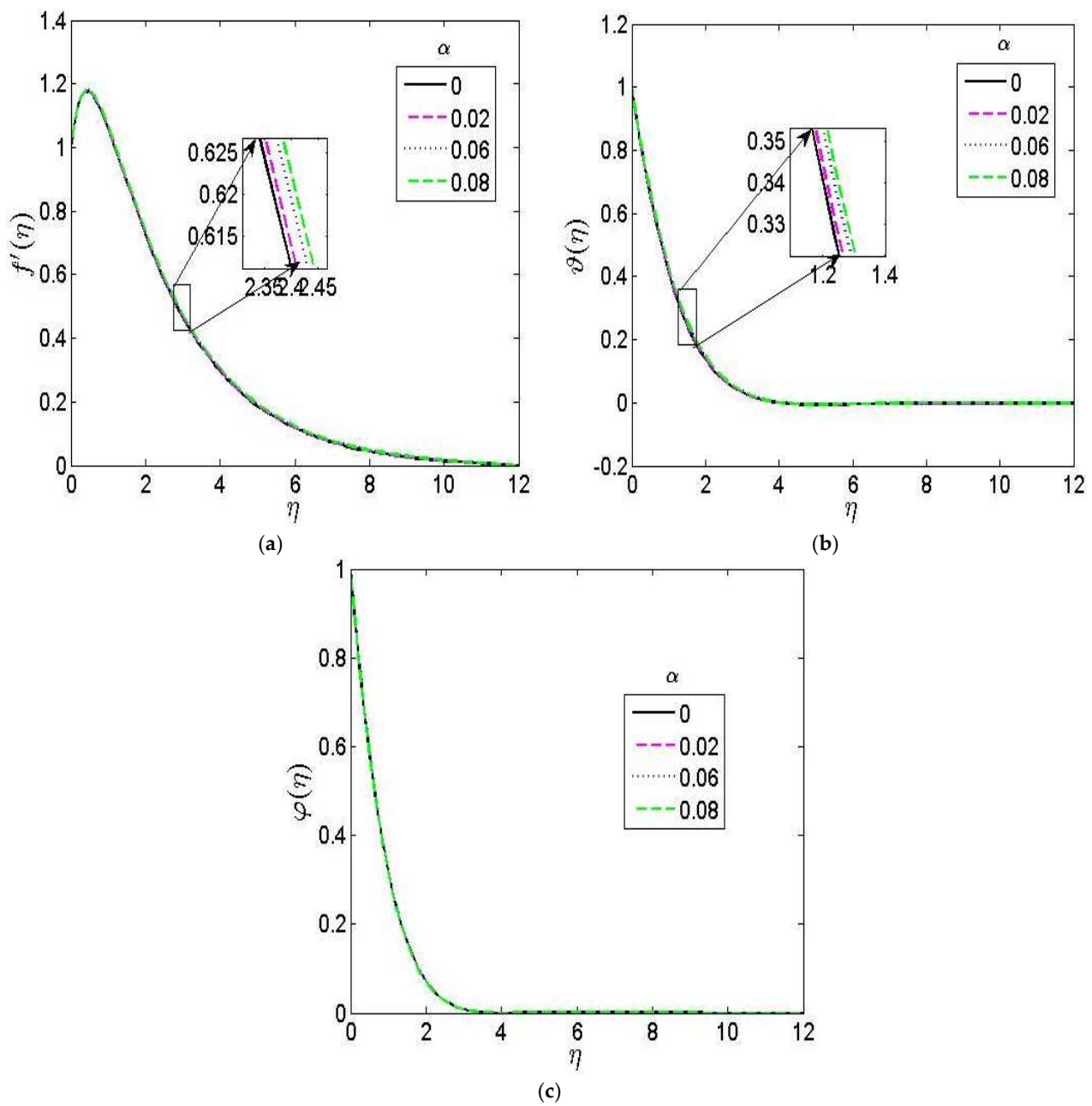


Figure 11. Effect of heat generation parameter α on (a) velocity, (b) temperature, and (c) concentration profiles.

The contribution of the thermal Grashof number (Gt) is elucidated in Figure 12. Gt defined the ratio of the force of buoyancy to that of viscous material affecting the liquid. The thermal Grashof number can also be called the thermal buoyancy force term. As expected, in Figure 12a. the fluid velocity elevates as the thermal buoyancy force parameter is intensified. Furthermore, from Figure 12b, the temperature field decreases with a higher value of thermal Grashof. It is interesting to observe a slight degeneration in the concentration field when Gt is increased.

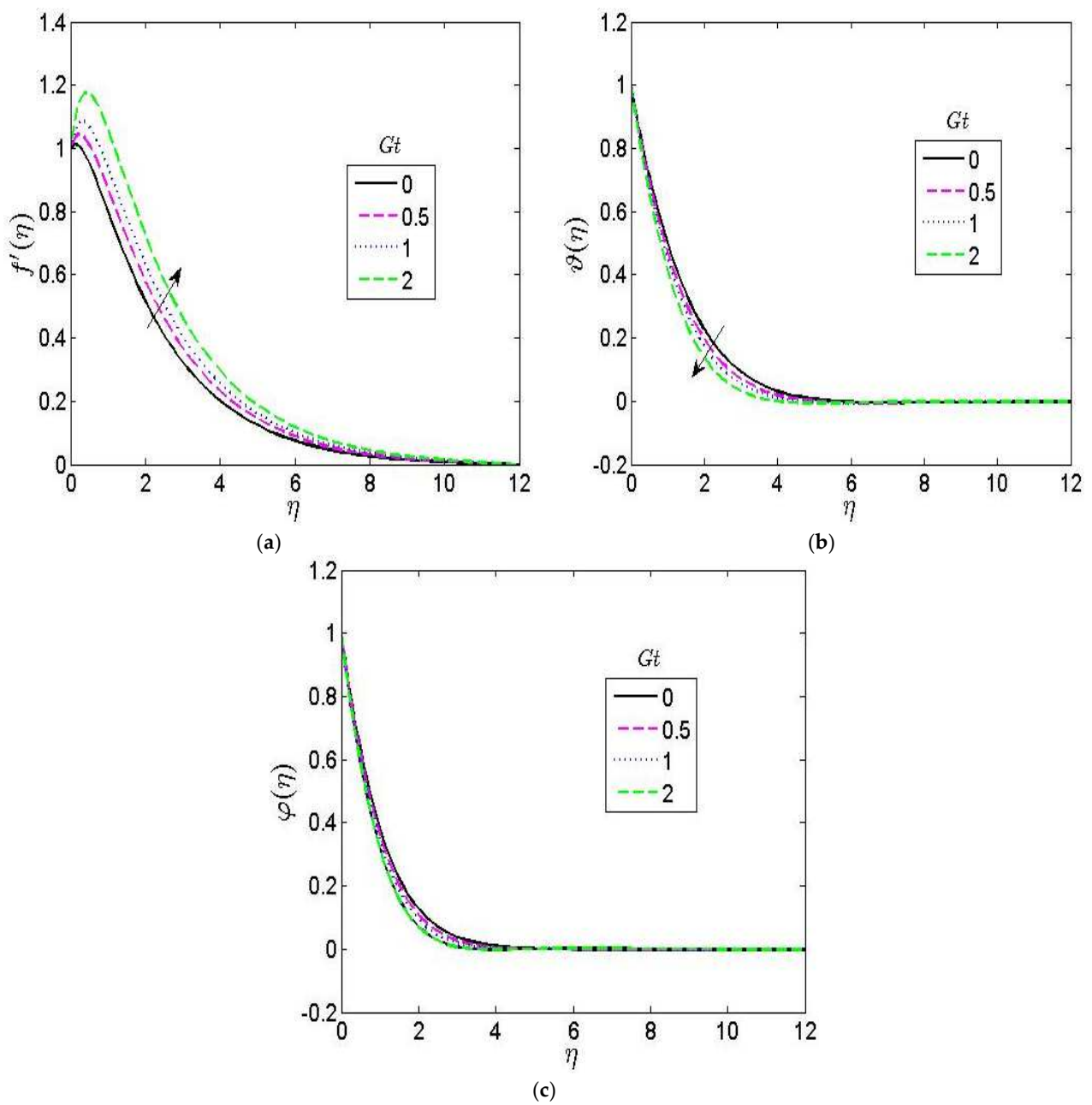


Figure 12. Effect of thermal Grashof number Gt on (a) velocity, (b) temperature, and (c) concentration profiles.

Figure 13 represents the effect of the mass Grashof number (Gm) on the velocity, concentration, and temperature graphs. In Figure 13a, it is discovered that an increment in the Gm number allows a rise in the velocity of the fluid. In the same vein, as seen in Figure 13b,c a higher mass Grashof decreases both the temperature and concentration.

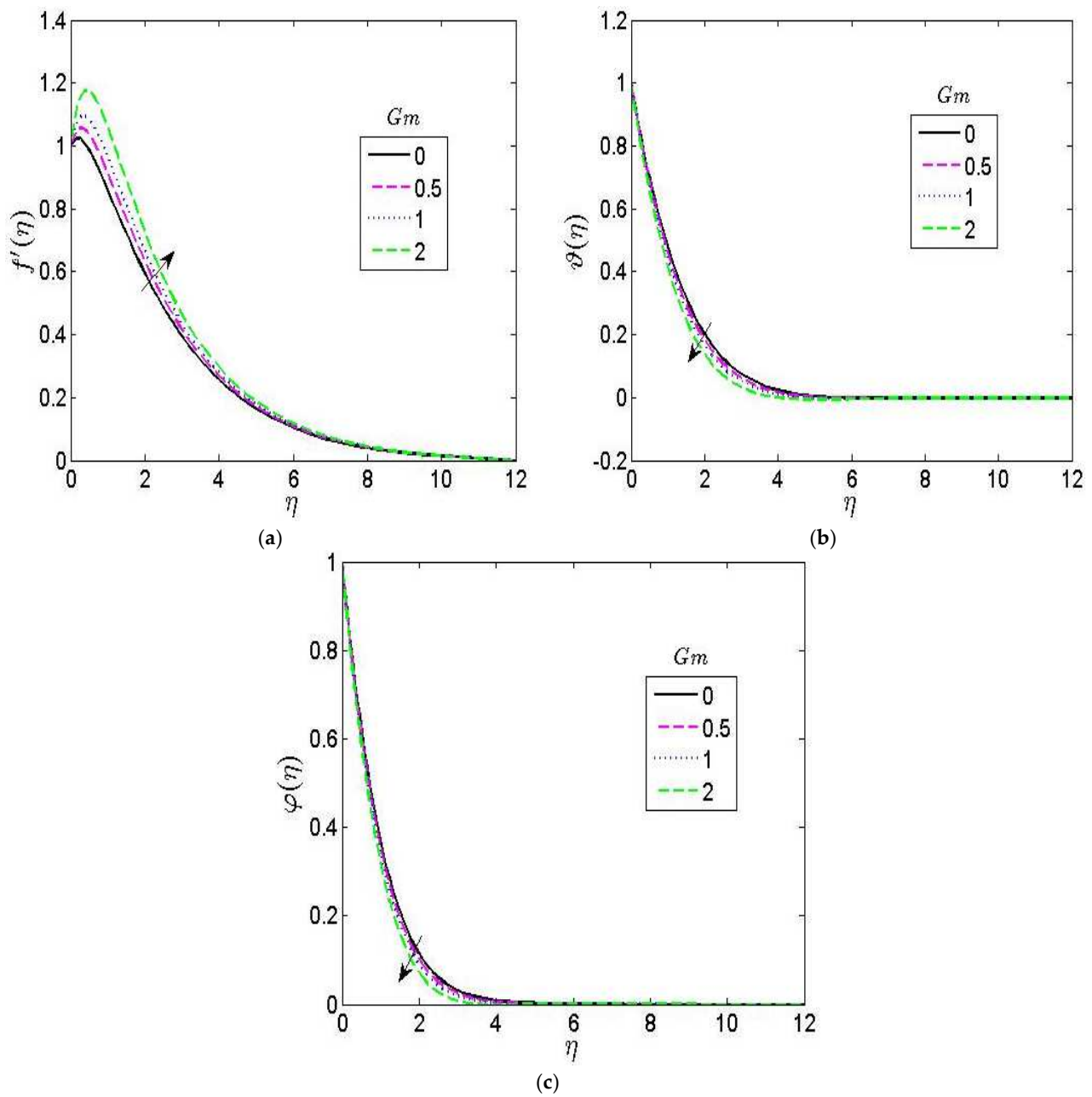


Figure 13. Effect of mass Grashof number G_m on (a) velocity, (b) temperature, and (c) concentration profiles.

Table 1 shows the numeric local skin friction, local Nusselt (Nu), and local Sherwood number (Sh). For distinct values of the viscoelastic parameter (β) and thermal Grashof number (Gt), they produce a notable elevation in the skin friction, local Nusselt, and local Sherwood numbers, respectively. In Table 2, we present the numeric local skin friction, local Nusselt, and Sherwood numbers for distinct values of the heat generation parameter (α) and Soret number (Sr). The results in Table 2 revealed that an increase in both heat generation α and the Soret number causes an increase in the skin friction, Nusselt, and Sherwood numbers.

Table 1. Numeric values of local skin friction, local Nusselt, and local Sherwood numbers for distinct values of viscoelastic parameter (β) and thermal Grashof number when $M = 1.0$, $R = 0.5$, $Pr = 0.71$, $E = 0.01$, $S_w = 0.1$, $\alpha = 0.01$, $Sr = 0.2$, $Df = 0.3$, $Sc = 0.61$.

β	Gt	Cf	Nu	Sh
0.0	0	0.35362	0.65313	0.92109
	0.5	0.53971	0.67986	0.94349
	1	0.72152	0.70418	0.96415
	2	1.07430	0.74707	1.001256
0.01	0	0.35618	0.65291	0.92095
	0.5	0.54379	0.67981	0.94351
	1	0.72714	0.70430	0.96431
	2	1.08301	0.74750	1.00168
0.05	0	0.36766	0.65211	0.92051
	0.5	0.56172	0.67975	0.94369
	1	0.75155	0.70493	0.96508
	2	1.12046	0.74942	1.00358

Table 2. Numeric values of local skin friction, local Nusselt, and local Sherwood numbers for distinct values of heat generation parameter (α) and Soret number (Sr) when $M = 1.0$, $R = 0.5$, $Pr = 0.71$, $E = 0.01$, $S_w = 0.1$, $Sr = 0.2$, $Df = 0.3$, $Sc = 0.61$.

α	Sr	$\beta = 0, Sw = 0.02$			$\beta = 0.01, Sw = 0.06$		
		Cf	Nu	Sh	Cf	Nu	Sh
0.0	0	1.09417	0.70364	1.01421	1.05091	0.74833	1.06656
	0.5	1.13712	0.74918	0.88981	1.09354	0.79586	0.92930
	1	1.18712	0.80057	0.74683	1.14279	0.84920	0.77128
	2	1.31471	0.92566	0.38704	1.26665	0.97771	0.37455
0.02	0	1.09968	0.69008	1.01670	1.05523	0.73602	1.06848
	0.5	1.14095	0.73666	0.89450	1.09652	0.78449	0.93333
	1	1.18941	0.78945	0.75314	1.14456	0.83905	0.77707
	2	1.31473	0.91886	0.39461	1.26665	0.97114	0.38196
0.08	0	1.11955	0.64363	1.02623	1.06975	0.69593	1.07521
	0.5	1.15414	0.69539	0.91000	1.10609	0.74877	0.94608
	1	1.19652	0.75529	0.77245	1.14970	0.80902	0.79406
	2	1.31363	0.90744	0.40934	1.26587	0.95815	0.39801

5. Conclusions

This study presents the numerical outcomes of the MHD free convective motion of Walters-B liquid past a permeable accelerating surface with the contribution of Soret and Dufour. The equations of motion PDEs, which modeled the problem under investigation, were evaluated into fourth-order coupled and highly nonlinear total differential equations with suitable similarity functions. We solved the transformed fourth-order coupled and highly nonlinear ordinary differential equations in Equations (19)–(21) using SHAM. SHAM uses the traditional HAM in conjunction with the Chebyshev pseudospectral method to solve differential equations. Spectral methods are now an essential instrument for scientist and engineers to solve complex problems. Detailed explanations of SHAM are presented in the previous section.

The present results show that the application of magnetism gives rise to a drag-like force (i.e., Lorentz force), thereby lowering the fluid velocity. This study also explains the application of the MHD flow of viscoelastic fluid in biomechanics, the petroleum industry, etc. The present results reveal that the velocity decreases drastically with an increase in the viscoelastic parameter (β). Furthermore, this study shows that an increase in the Dufour parameter intensifies the fluid velocity alongside temperature. This is owing to the energy flux, which rises due to the concentration gradient, which is inversely proportional to the velocity. In the same vein, a higher Soret term increases the velocity and concentration field.

Finally, the influence of Soret, Dufour, thermal radiation, and heat generation/absorption on the flow region is significant and thereby finds application in diverse problems in engineering such as isotope separation, nuclear waste disposal, petroleum reservoirs, etc.

Author Contributions: Conceptualization, P.A., M.N.S.S., V.V.V.M., C.S.C., V.V.S., K.K.S., D.S.A.-Z., E.L., C.P., D.B. and R.C.; Data curation, P.A., M.N.S.S., V.V.V.M., C.S.C., V.V.S., K.K.S., D.S.A.-Z., E.L., C.P., D.B. and R.C.; Formal analysis, P.A., M.N.S.S., V.V.S., E.L., C.P., D.B. and R.C.; Funding acquisition, P.A. and C.P.; Investigation, P.A., M.N.S.S., V.V.V.M., C.S.C., V.V.S., K.K.S., D.S.A.-Z., E.L., C.P., D.B. and R.C.; Methodology, P.A., M.N.S.S., V.V.V.M., C.S.C., K.K.S., E.L., C.P., D.B. and R.C.; Project administration, R.C.; Resources, P.A.; Supervision, P.A., D.S.A.-Z., D.B. and R.C.; Validation, P.A. and V.V.V.M.; Visualization, P.A. and V.V.S.; Writing—original draft, P.A., M.N.S.S., V.V.V.M., C.S.C., V.V.S., E.L., C.P., D.B. and R.C.; Writing—review & editing, K.K.S., D.S.A.-Z., E.L., C.P., D.B. and R.C. All authors have read and agreed to the published version of the manuscript.

Funding: This research was funded by a grant of the Romanian Ministry of Research, Innovation and Digitalization, project number PFE 26/30.12.2021, PERFORM-CDI@UPT100—The increasing of the performance of the Polytechnic University of Timișoara by strengthening the research, development and technological transfer capacity in the field of “Energy, Environment and Climate Change” at the beginning of the second century of its existence, within Program 1—Development of the national system of Research and Development, Subprogram 1.2—Institutional Performance—Institutional Development Projects—Excellence Funding Projects in RDI, PNCDI III.

Institutional Review Board Statement: Not applicable.

Informed Consent Statement: Not applicable.

Data Availability Statement: Not applicable.

Conflicts of Interest: The authors declare no conflict of interest.

Nomenclature

u	x -axis velocity component (Unit: m/s)
v	y -axis component (Unit: m/s)
g	gravity
D	diffusivity
β_0	Constant magnetism
c_p	specific heat (Unit: J/kgk)
q_r	radiative heat flux (Unit: W/m ²)
k_T	Ratio of thermal diffusion
c_s	concentration susceptibility
T_w	Temperature (Unit: K)
C_w	concentration
k_0	viscoelastic term
Q_0	heat generation term
k_s	absorption coefficient
σ^*	Stefan-Boltzman
β_t, β_c	Thermal expansion and concentration, respectively
α	Angle of inclination (Unit: degree)
θ	Dimensionless temperature (Unit: K)
φ	Dimensionless concentration
T_∞	temperature far from layers (Unit: K)
C_∞	Concentration far from layers (Unit: mol)
σ	electrical conductivity
ρ	Density of liquid (Unit: kg/m ³)
ν	Viscosity of liquid (Unit: m ² /s)
ψ	stream relations (Unit: m ² /s)
η	Distance variable (Unit: dimensionless)

References

1. Alam, M.S.; Rahman, M.M.; Samad, M.A. Dufour and Soret Effects on Unsteady MHD Free Convection and Mass Transfer Flow past a Vertical Porous Plate in a Porous Medium. *Nonlinear Anal. Model. Control* **2006**, *11*, 217–226. [[CrossRef](#)]
2. Mahdy, A. Non-Darcy non-newtonian free convection flow over a vertical plate under the influence of Soret and Dufour effect. *Int. J. Appl. Mech. Eng.* **2008**, *13*, 1125–1132.
3. Makinde, O.D. On MHD convection with Soret and Dufour effects past a vertical plate embedded in a porous medium. *Lat. Am. Appl. Res.* **2011**, *41*, 63–68.
4. Cheng, C.-Y. Soret and Dufour Effects on Mixed Convection Heat and Mass Transfer from a Vertical Wedge in a Porous Medium with Constant Wall Temperature and Concentration. *Transp. Porous Media* **2012**, *94*, 123–132. [[CrossRef](#)]
5. Moorthy, M.B.K.; Senthilvadivu, K. Soret and Dufour Effects on Natural Convection Flow Past a Vertical Surface in a Porous Medium with Variable Viscosity. *J. Appl. Math.* **2012**, *2012*, 1–15. [[CrossRef](#)]
6. Sharma, B.K.; Yadav, K.; Mishra, N.K.; RChavdhary, C. Soret and Dufour effects on unsteady MHD mixed convection flow past a radiative vertical porous plate embedded in a porous medium with chemical reaction. *Appl. Math.* **2012**, *2012*, 717–723. [[CrossRef](#)]
7. Seini, Y.I.; Makinde, O.D. Hydromagnetic flow with Dufour and Soret effect past a vertical plate embedded in porous medium. *Math. Theory Model.* **2013**, *3*, 2224–5804.
8. Uwanta, I.J.; Usman, H. On the influence of Soret and Dufour effects on MHD free convective heat and mass transfer flow over a vertical channel with constant suction and viscous dissipation. *Sch. Res. Not.* **2014**, *2014*, 11. [[CrossRef](#)]
9. Aruna, G.; Varma, S.V.; Raju, R.S. Combined influence of Soret and Dufour effect on unsteady hydromagnetic mixed convective flow in an accelerated vertical wavy plate through a porous medium. *Int. J. Adv. Appl. Math. Mech.* **2015**, *3*, 122–134.
10. Tella, H.; Vijaykumar, P.; Naidu, A. Homotopy analysis to Soret and Dufour effects on heat and mass transfer chemically reacting fluid past a moving vertical plate with viscous dissipation. *IOSR J. Math.* **2015**, *11*, 106–121.
11. Joneidi, A.A.; Domairry, G.; Babalahi, M. Homotopy Analysis Method to Walter's B fluid in a vertical channel with porous wall. *Meccanica* **2010**, *45*, 857–868. [[CrossRef](#)]
12. Kumar, A. Mathematical Study of Thermosolutal Convection in Heterogeneous Viscoelastic Fluid in the Presence of Porous Medium. *Am. J. Math. Anal.* **2017**, *5*, 12–16.
13. Vijaya, R.B.; Gaffar, S.A.; Venkatadri, K.; Khan, B.m.h. Flow and Thermal Convection of Third Grade Viscoelastic Fluid from a Vertical Porous Plate with Biot Number Effects. *Int. J. Math. Arch.* **2017**, *2017*, 109–125.
14. Pandey, S.D.; Nema, V.K.; Tiwari, S. Characteristic of Walter's B Visco-elastic Nanofluid Layer Heated from Below. *Int. J. Energy Eng.* **2016**, *6*, 7–13.
15. Moatimid, G.M.; Hassan, M.A. Convection instability of non-Newtonian Walter's nanofluid along a vertical layer. *J. Egypt. Math. Soc.* **2017**, *25*, 220–229. [[CrossRef](#)]
16. Islam, M.M.; Haque, M. Radiative Walter's memory flow along a vertical cone in induced magnetic field with thermophoretic effect. *AIP Conf. Proc.* **1851**, 020015. [[CrossRef](#)]
17. Rana, G.C.; Chand, R. Rayleigh-Benard Convection in an Elastico-viscous Walters' (Model B') Nanofluid Layer. *Bull. Pol. A Acad. Sci. Tech. Sci.* **2015**, *63*, 2015. [[CrossRef](#)]
18. Hayat, T.; Hussain, Z.; Alsaedi, A. Influence of heterogeneous-homogeneous reactions in thermally stratified stagnation point flow of an Oldroyd-B fluid. *Results Phys.* **2016**, *6*, 1161–1167. [[CrossRef](#)]
19. Moorthy, M.B.K.; Kannan, T.; Senthilvadivu, K.; Rangasamy, K.S. Soret and Dufour effects on natural convection heat and mass transfer flow past a horizontal surface in a porous medium with variable viscosity. *WSEAS Trans. Heat Mass Transf.* **2013**, *8*, 2224–3461.
20. Lavanya, B.; Ratnam, A.L. Dufour and Soret effects on steady MHD free convective flow past a vertical porous plate embedded in a porous medium with chemical reaction, radiation heat generation an viscous dissipation. *Adv. Appl. Sci. Res.* **2014**, *5*, 127–142.
21. Reddy, G.V.R.; Subrahmanyam, S.V.; Satishkumar, d. Soret effect on MHD mixed convection oscillatory flow over a vertical surface in a porous medium with chemical reaction and thermal radiation. *Ultra Sci.* **2014**, *26*, 49–60.
22. Krishna, P.M.; Vidyasagar, G.; Sandeep, N.; Sugunamma, V. Soret and Dufour effect on MHD free convective flow over a permeable stretching surface with chemical reaction and heat source. *Int. J. Sci. Eng. Res.* **2015**, *6*, 143–147.
23. Srinivasacharya, D.; Mallikarjuna, B.; Bhuvanavijaya, R. Soret and Dufour effect of mixed convection along a vertical wavy surface in a porous medium with variable properties. *Ain Shams Eng. J.* **2015**, *6*, 553–564. [[CrossRef](#)]
24. Motsa, S.S.; Sibanda, P.; Shateyi, S. A New Spectral Homotopy Analysis Method for Solving a Nonlinear Second Order BVP. *Commun. Nonlinear Sci. Numer. Simul.* **2010**, *15*, 2293–2302. [[CrossRef](#)]
25. Zhang, G.; Zhang, Z.; Sun, M.; Yu, Y.; Wang, J.; Cai, S. The Influence of the Temperature on the Dynamic Behaviors of Magnetorheological Gel. *Adv. Eng. Mater.* **2022**, 2101680. [[CrossRef](#)]
26. Motsa, S.S.; Awad, F.G.; Makukula, Z.G.; Sibanda, P. The Spectral Homotopy Analysis Method Extended to Systems of Partial Differential Equations. *Abstr. Appl. Anal.* **2014**, *2014*, 1–11. [[CrossRef](#)]
27. Motsa, S.S.; Makukula, Z.G. On a Bivariate Spectral Homotopy Analysis Method for Unsteady Mixed Convection Boundary Layer Flow, Heat, and Mass Transfer due to a Stretching Surface in a Rotating Fluid. *J. Appl. Math.* **2017**, *2017*, 1–15. [[CrossRef](#)]

28. Fagbade, A.; Falodun, B.; Omowaye, A. MHD natural convection flow of viscoelastic fluid over an accelerating permeable surface with thermal radiation and heat source or sink: Spectral Homotopy Analysis Approach. *Ain Shams Eng. J.* **2018**, *9*, 1029–1041. [[CrossRef](#)]
29. Motsa, S.S.; Marewo, G.T.; Sibanda, P.; Shateyi, S. An improved spectral homotopy analysis method for solving boundary layer problems. *Bound. Value Probl.* **2011**, *2011*, 3–9. Available online: <http://www.boundaryvalueproblems.com/content/2011/1/3> (accessed on 10 July 2022). [[CrossRef](#)]
30. Yang, S.; Li, X.; Yu, T.; Wang, J.; Fang, H.; Nie, F.; He, B.; Zhao, L.; Lü, W.; Yan, S. High-Performance Neuromorphic Computing Based on Ferroelectric Synapses with Excellent Conductance Linearity and Symmetry. *Adv. Funct. Mater.* **2022**, *32*, 2202366. [[CrossRef](#)]
31. Fagbade, A.I.; Falodun, B.O.; Boneze, C.U. Influence of Magnetic Field, Viscous Dissipation and Thermophoresis on Darcy-Forcheimer Mixed Convection Flow in Fluid Saturated Porous Media. *Am. J. Comput. Math.* **2015**, *05*, 18–40. [[CrossRef](#)]
32. Mehmood, A.; Ali, A.; Shah, T. Heat transfer analysis of unsteady boundary layer flow by homotopy analysis method. *Commun. Nonlinear Sci. Numer. Simul.* **2008**, *13*, 902–912. [[CrossRef](#)]
33. Walter, K. Non-Newtonian effects in some elastico-viscous liquids whose behavior at some states of shear is characterized by general equation of state. *Q. J. Mech. Appl. Math.* **1962**, *15*, 63–76. [[CrossRef](#)]
34. Liao, S.J. *Beyond Perturbation: Introduction to the Homotopy Analysis Method*; Chapman and Hall/CRC Press: Boca Raton, FL, USA, 2003.
35. Canuto, C.; Hussaini, M.Y.; Quarteroni, A.; Zang, T.A. *Spectral Methods in Fluid Dynamics*; Springer: Verlag/Berlin, Germany, 1988.
36. Fornberg, B. *A Practical Guide to Pseudospectral Methods*; Cambridge Univ. Press: New York, NY, USA, 1996.
37. Trefethen, L.N. *Spectral Methods in MATLAB*; SIAM: Philadelphia, PA, USA, 2000.
38. Sun, L.; Wang, G.; Zhang, C.; Jin, Q.; Song, Y. On the rheological properties of multi-walled carbon nano-polyvinylpyrrolidone/silicon-based shear thickening fluid. *Nanotechnol. Rev.* **2021**, *10*, 1339–1348. [[CrossRef](#)]
39. Ullah, A.; Ikramullah; Selim, M.M.; Abdeljawad, T.; Ayaz, M.; Mlaiki, N.; Ghafoor, A. A Magnetite–Water-Based Nanofluid Three-Dimensional Thin Film Flow on an Inclined Rotating Surface with Non-Linear Thermal Radiations and Couple Stress Effects. *Energies* **2021**, *14*, 5531. [[CrossRef](#)]
40. Khan, S.; Selim, M.; Khan, A.; Ullah, A.; Abdeljawad, T.; Ikramullah; Ayaz, M.; Mashwani, W. On the Analysis of the Non-Newtonian Fluid Flow Past a Stretching/Shrinking Permeable Surface with Heat and Mass Transfer. *Coatings* **2021**, *11*, 566. [[CrossRef](#)]
41. Zhang, G.; Chen, J.; Zhang, Z.; Sun, M.; Yu, Y.; Wang, J.; Cai, S. Analysis of magnetorheological clutch with double cup-shaped gap excited by Halbach array based on finite element method and experiment. *Smart Mater. Struct.* **2022**, *31*, 075008. [[CrossRef](#)]
42. Nawaz, R.; Hussain, Z.; Khattak, A.; Khan, A. Extension of Optimal Homotopy Asymptotic Method with Use of Daftardar–Jeffery Polynomials to Coupled Nonlinear-Korteweg–De-Vries System. *Complexity* **2020**, *2020*, 1–6. [[CrossRef](#)]
43. Shah, Z.; Kumam, P.; Ullah, A.; Khan, S.N.; Selim, M.M. Mesoscopic Simulation for Magnetized Nanofluid Flow Within a Permeable 3D Tank. *IEEE Access* **2021**, *9*, 135234–135244. [[CrossRef](#)]